AD-A107 730   RCA LABS PRINCETON NJ   F/G 20/6
                FABRICATION OF HETEROJUNCTION LEDS FOR OPERATION AT 1.3 MICROME--ETC(U)
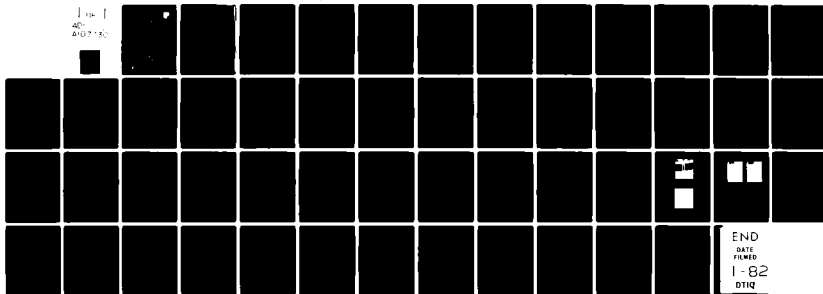   SEP 81   G H OLSEN, F Z HAWRYLO, D J CHANNIN   F19628-79-C-0115
UNCLASSIFIED   PRRL-80-CR-35   RADC-TR-81-199   NL

END
DATE
FILMED
1-82
DTIC

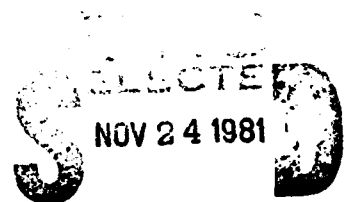LEVEL II (12)

RADC-TR-81-199
Final Technical Report
September 1981

FABRICATION OF HETEROJUNCTION LEDs FOR OPERATION AT 1.3 μm

RCA Laboratories

G. H. Olsen
F. Z. Hawrylo
D. J. Channin
D. Botez
M. Ettenberg

AD A107730

APPROVED FOR PUBLIC RELEASE; DISTRIBUTION UNLIMITED

SELECTED
NOV 24 1981

A

ROME AIR DEVELOPMENT CENTER
Air Force Systems Command
Griffiss Air Force Base, New York 13441

DTIC FILE COPY

81 11 24 047

This report has been reviewed by the RADC Public Affairs Office (PA) and is releasable to the National Technical Information Service (NTIS). At NTIS it will be releasable to the general public, including foreign nations.

RADC-TR-81-199 has been reviewed and is approved for publication.

APPROVED: *[signature]*

D. EIRUG DAVIES
Project Engineer

APPROVED: *[signature]*

FREEMAN D. SHEPHERD, Jr.
Acting Director, Solid State Sciences Division

FOR THE COMMANDER: *[signature]*

JOHN P. HUSS
Acting Chief, Plans Office

If your address has changed or if you wish to be removed from the RADC mailing list, or if the addressee is no longer employed by your organization, please notify RADC.(ESO)Hanscom AFB MA 01731. This will assist us in maintaining a current mailing list.

Do not return copies of this report unless contractual obligations or notices on a specific document requires that it be returned.

SECURITY CLASSIFICATION OF THIS PAGE *(When Data Entered)*

REPORT DOCUMENTATION PAGE		READ INSTRUCTIONS BEFORE COMPLETING FORM
1. REPORT NUMBER RADC-TR-81-199	2 GOVT ACCESSION NO. AD-A107 730	3. RECIPIENT'S CATALOG NUMBER
4. TITLE *(and Subtitle)* FABRICATION OF HETEROJUNCTION LEDs FOR OPERATION AT 1.3 μm		5. TYPE OF REPORT & PERIOD COVERED Final Technical Report 15 Jun 79 - 14 Jun 80
		6. PERFORMING ORG. REPORT NUMBER PRRL-80-CR-35
7. AUTHOR(s) G. H. Olsen, F. Z. Hawrylo, D. J. Channin, D. Botez and M. Ettenberg		8. CONTRACT OR GRANT NUMBER(s) F19628-79-C-0115
9. PERFORMING ORGANIZATION NAME AND ADDRESS RCA Laboratories Princeton NJ 08540		10. PROGRAM ELEMENT. PROJECT. TASK AREA & WORK UNIT NUMBERS 62702F 46001931
11. CONTROLLING OFFICE NAME AND ADDRESS Deputy for Electronic Technology (RADC/ESO) Hanscom AFB MA 01731		12. REPORT DATE September 1981
		13. NUMBER OF PAGES 52
14. MONITORING AGENCY NAME & ADDRESS*(if different from Controlling Office)* Same		15. SECURITY CLASS. *(of this report)* UNCLASSIFIED
		15a. DECLASSIFICATION/DOWNGRADING SCHEDULE N/A
16. DISTRIBUTION STATEMENT *(of this Report)* Approved for public release; distribution unlimited.		
17. DISTRIBUTION STATEMENT *(of the abstract entered in Block 20, if different from Report)* Same		
18. SUPPLEMENTARY NOTES RADC Project Engineer: D. Eirug Davies (RADC/ESO)		
19. KEY WORDS *(Continue on reverse side if necessary and identify by block number)* LED InGaAsP Liquid-phase epitaxy Vapor-phase epitaxy Fiber coupling		

20. ABSTRACT *(Continue on reverse side if necessary and identify by block number)*

This report describes research undertaken to study and optimize the device properties of 1.3-μm InGaAsP edge-emitting LEDs fabricated by both vapor-phase epitaxy (VPE) and liquid-phase epitaxy (LPE). Edge-emitting LEDs have been prepared with both growth methods with a combination of properties rivaling the best reported to date. In the previous final report (RADC-TR-80-110) details of the VPE growth process were presented. Details of the LPE growth process are presented here. The LED efficiency—

(Cont'd)

DD FORM, JAN 73, 1473   EDITION OF 1 NOV 65 IS OBSOLETE

Item 20 (Cont'd)

of LPE devices was found to increase with decreasing cavity thickness. A value over 1% was measured with a 1000 Å.

Contact stripe width and coupling technique were also varied to achieve maximum power into an optical fiber. The best coupling was obtained with a 12-μm-wide contact stripe. Significantly better coupling was also achieved with a balled, rather than cleaved, end fiber. More than twice the power could be coupled into a 100-μm core diameter fiber, as compared to a 50-μm core fiber.

The temperature dependence of LED emission was also measured for both VPE and LPE devices. LED efficiency dropped over 30% between 20^0 and 70^0C, while an emission wavelength shift of 5 to 6 Å/^{0}C was observed over the same temperature range.

Comparable results have now been achieved with both LPE and VPE devices.

Highlights include typical coupled power into fibers of 40 μW (Best: 135 μW), spectral half-widths $\sim$600 Å, rise/fall times $\sim$3 ns, ac modulation rates 100 to 200 MHz and reliability (determined under separate government-sponsored programs) of >14,000 h at 70^0C (VPE) and >3000 h at 120^0C (LPE).

Far-field patterns from InGaAsP/InP were found to contain asymmetries due to the lack of absorbing substrate and cap layers. Some narrowing was achieved via the use of thin (1000-Å) active regions. Unusual effects upon far-field patterns were also observed when highly absorbing (i.e., low-bandgap) materials were incorporated into the device structures.

A refractive index step $\Delta n = 0.28$ was estimated for 1.3-μm InGaAsP/InP lattice-matched interfaces from far-field pattern half-widths. This value is in good agreement with other experimental and calculated values.

PREFACE

This Final Report was prepared at RCA Laboratories, Princeton, New Jersey, during the period 15 June 1979 through 14 June 1980, under Contract No. F19628-79-C-0115. The program was carried out in the Solid State Devices Laboratory, directed by Dr. B. Hershenov. Dr. M. Ettenberg, Group Head of Optoelectronic Devices and Systems Research, will supervise the project. Dr. G. H. Olsen is the Project Scientist. Other staff members who contributed to this program are Mr. F. Z. Hawrylo, Dr. D. J. Channin, and Dr. D. Botez.

TABLE OF CONTENTS

LIST OF ILLUSTRATIONS

LIST OF ILLUSTRATIONS (Continued)

LIST OF TABLES

I. LPE TECHNIQUE

The LPE technique employed for the growth of InGaAsP/InP LEDs described here is the single-phase supercooling method similar to that described by Hsieh [1]. The solution components are carefully weighed and heated to a temperature at which a saturated solution is obtained. The equilibrium melt composition can be determined by observing the solution through a semitransparent gold reflector furnace. A thermocouple is suspended in the solution (see experimental configuration in Fig. 1). The temperature is lowered until crystals just begin to precipitate on the solution surface. The temperature is then raised in 0.1°C increments until complete dissolution of the crystals is observed. This temperature determines the equilibrium liquidus-solidus temperature for the given melt composition.

A typical growth schedule for a double-heterostructure LED is shown in Fig. 2 (which contains a sketch of the substrate and solutions, together with a plot of solution temperature vs time) and Table 1 (which lists the detailed melt compositions, segregation coefficients, and growth times). The furnace is first increased in temperature to 655°C and maintained for one hour to homogenize the solutions in which the InP substrate resides in a H_2 atmosphere. Decomposition of the substrate, due to preferential phosphorus evaporation, undoubtedly takes place. The furnace is then cooled from 655°C at a rate of ~0.27°C/min. When the temperature drops to 650°C, the substrate is pulled into a pure indium solution (bin 1) for 5 s to meltback or dissolute the damaged surface of the substrate. The wafer is then sequentially pulled through bins 2 to 5 to grow the subsequent layers described in Table 1 (bin 5 actually contains p-InGaAsP "cap-layer" melt constituents). After the structure is grown, oxide-stripe edge-emitting LEDs are fabricated as described in the final report for the previous year of this contract. Lattice parameters for all four epitaxial layers can then be obtained for x-ray diffraction. The bandgap of the p-InGaAsP layer is determined by photoluminescence, whereas the cavity bandgap is determined approximately from the spontaneous emission spectra.

1. J. J. Hsieh, Appl. Phys. Lett. 28, 283 (1976).
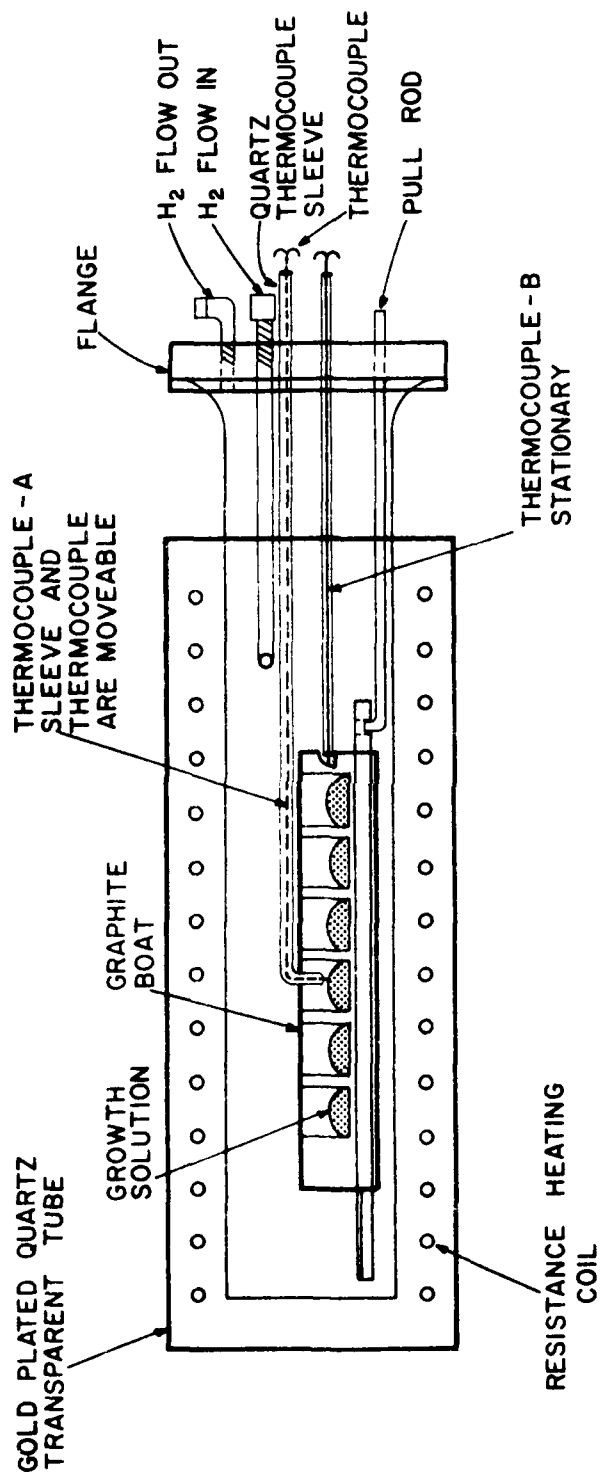
Figure 1. Sketch of graphite boat used for LPE growths.

GOLD PLATED QUARTZ
TRANSPARENT TUBE

THERMOCOUPLE - A
SLEEVE AND
THERMOCOUPLE
ARE MOVEABLE

GRAPHITE
BOAT

GROWTH
SOLUTION

RESISTANCE HEATING
COIL

THERMOCOUPLE - B
STATIONARY

FLANGE

H₂ FLOW OUT
H₂ FLOW IN

QUARTZ
THERMOCOUPLE
SLEEVE

THERMOCOUPLE

PULL ROD

2

SINGLE PHASE, SUPERCOOLING

MELT

SUBSTRATE

(T)
655°C
650°C
635°C

0.2 °C/min

PULL-IN

START
QUATERNARY
GROWTH

0   60   90

MINUTES
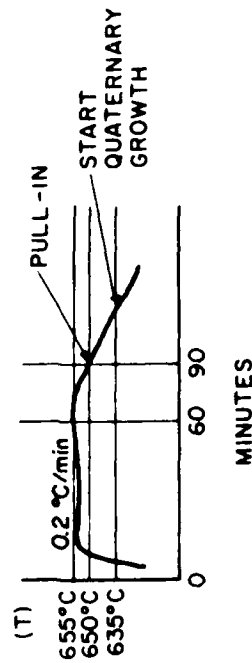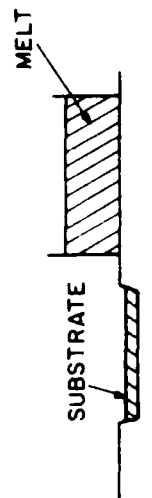
COMMENTS

1) PHOSPHORUS LOSS COMPENSATED
   BY EXCESS IN MELT

2) NO PRECIPITATION ANYWHERE
   EXCEPT ON SUBSTRATE

3) MAXIMUM SUPERCOOLING

TWO PHASE, SUPERCOOLING

TOP InP WAFERS

MELT

SUBSTRATE

(T)
675°C
655°C
635°C

0.5 °C/min

PULL-IN

START
QUATERNARY
GROWTH

0   60   100

MINUTES
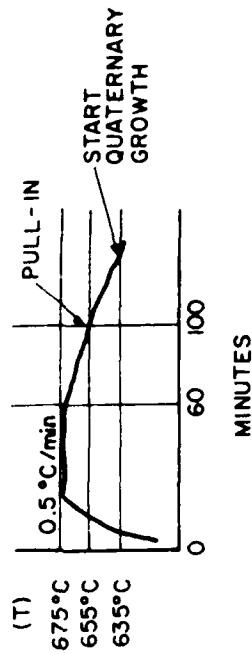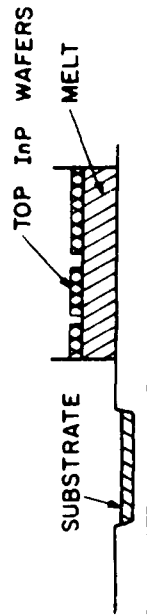
COMMENTS:

1) PHOSPHORUS LOSS SELF-COMPENSATED

2) PRECIPITATION TOP AND SUBSTRATE

3) LIMITED SUPERCOOLING

Figure 2. Growth schedule (temperature-time profile for LPE growths).

3

TABLE 1. MELT, SOLID, AND GROWTH PARAMETERS FOR THE FABRICATION OF AN InGaAsP/InP LED

| | Weight (mg) | | | | | |
	In	InP	InAs	GaAs	Sn	Zn
1. Wipeoff	4500					
2. n-InP	5000	48			60	
3. n-InGaAsP	4464	13.5	306	44.9		
4. p-InP	5000	42				0.1
5. p-InGaAsP	4500	9.7	327	65		1.0

| | Temp (°C) | Cooling Rate (°C/min) | Growth Time (seconds) | Solid Composition (alloy %) | | | | | Segregation Coefficient | | | | λ (μm) | $\Delta a/a$ (%) |
				In	Ga	As	P	P_{In}	P_{Ga}	P_{As}	P_p		
1. Wipeoff	650	0.27	5										
2. n-InP	650	0.27	3000	100			100						
3. n-InGaAsP	635	0.27	3	74.7	25.3	54.4	45.6	0.3948	17.605	6.1093	106.36	1.28	0
4. p-InP	635	0.27	600	100	28.1		100						
5. p-InGaAsP	632.3	0.27	10	71.9	28.1	67.6	32.4	0.3832	13.51	6.79	101.25	1.44	0.23

II. DEVICE RESULTS

A. LED RESULTS OBTAINED FROM LPE MATERIAL

During this contract much emphasis was placed on the growth and fabri-
cation of 1.3-μm LEDs grown by liquid-phase epitaxy (LPE), since such material
has demonstrated high external efficiency (η_{LED} 0.5% to 2.0%). Figure 3 contains
a plot of some recent results.
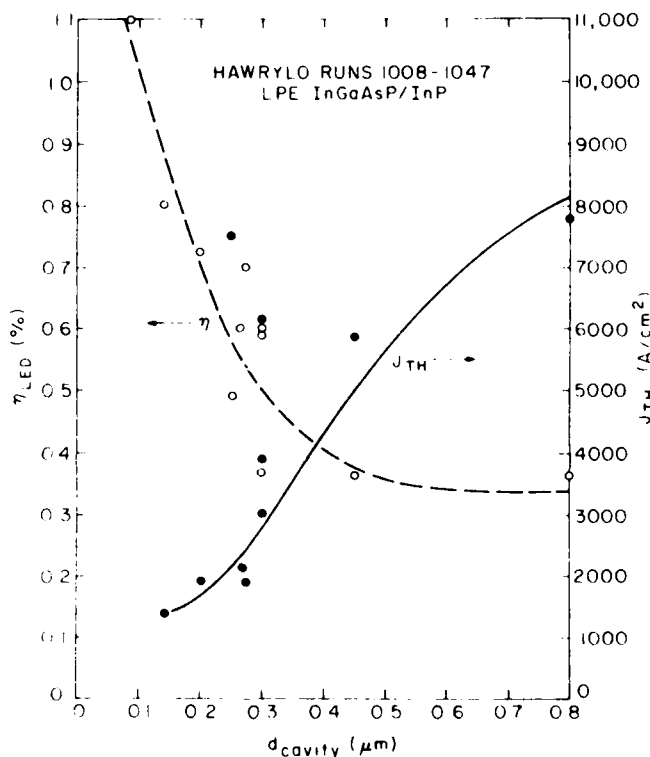
Figure 3. Measured LED power efficiency (n) and broad-area
lasing threshold current density vs cavity thick-
ness for InGaAsP/InP LED structures grown by LPE.

The broad-area pulsed lasing threshold was also measured as an indicator
of the material quality. Note how the lasing threshold current density steadily
decreases with cavity thickness whereas the LED efficiency steadily increases.

The lasing threshold current density is expected [2] to decrease with
thickness down to a minimum value and then increase again. Botez [3] has
calculated this minimum value to be between 1200 and 2000 Å for InGaAsP/InP

lasers (~1.3 μm) and for the threshold current density to vary only by ±10% for cavity thicknesses between 1000 and 3000 Å. Since in an edge-emitting LED the light is guided by the double heterojunction structure, the LED efficiencies are expected to increase with decreasing thickness and the power output has been shown [4] to vary as

$$P = P_o(1 - e^{\alpha L})/\alpha \qquad (1)$$

where
$$L = \text{LED length}$$
$$P_o = \text{output power in the absence of any absorption}$$
$$\alpha = \text{net absorption loss due to both the cavity}$$
$$\text{and confining layers} = \Gamma\alpha_A + (1-\Gamma)\,\alpha_W$$
$$\Gamma = \text{confinement factor}$$
$$\alpha_A = \text{absorption coefficient within the active region}$$
$$\alpha_W = \text{losses in the confining layers}$$

The radiation confinement factor (Γ) varies with cavity thickness (d) as [5]

$$\Gamma = \frac{\Gamma_o}{1+\Gamma_o} \qquad\qquad \Gamma_o \sim 2\pi_1^2(n_1^2 - n_2^2)\,(d/\lambda)^2 \qquad (2)$$

where
$$n_1 = \text{refractive index of the active layer}$$
$$n_2 = \text{refractive index of the confining layers}$$

A further refinement can be made by taking the facet reflectivity (R) into account [6]. Then the power varies as

$$P/P_o = \frac{(1-R)(1-e^{-\alpha L})}{\alpha L(1-Re^{-\alpha L})} \qquad (3)$$

2. D. Botez, IEEE J. Quantum Electron. QE-17 (1981).
3. D. Botez, Appl. Phys. Lett. 35, 57 (1979).
4. D. Botez, P. Zory, and M. J. Brady, Electron. Lett. 14, 716 (1978).
5. D. Botez, IEEE J. Quantum Electron. QE-14, 230 (1978).
6. H. Burkhard and K. Mause, Solid-State Electron. 21, 1551 (1978).

Thus, P can be expressed in terms of d. This expression gives a relative indication of how the LED efficiency should vary with cavity thickness as the net absorption losses of the device are varied.

Plots of relative output power (P/P_o) vs cavity thickness (Eq. 3) for various values of absorption (α_A and α_W) may be found in Fig. 4. Note that the confining layer loss term (α_W) has the greatest effect with very thin cavities, whereas the effect of the active region absorption is more pronounced as thickness is increased. Although it must be emphasized that the curves shown in Fig. 4 represent power which is guided by the LED structure and does not account for unguided light which leaks out through the confining layers, they do provide a useful indicator of how the output power (and, thus, LED efficiency) should vary with thickness.

The experimental data of LED efficiency vs cavity thickness shown in Fig. 3 can be fit best by the curve of P/P_o vs d (Fig. 4) when α_A = 200 or 300 cm^{-1} and α_W = 30 cm^{-1}. The variation of P/P_o vs d for α_A = 100 cm^{-1} is simply too gentle to fit the experimental data. This suggests that the cavity absorption for quaternary InGaAsP alloys might be higher than previously thought (100 cm^{-1}). Figure 4 also suggests that fairly large gains in LED efficiency might be obtained by lowering the doping (i.e., lowering the free-carrier absorption losses in α_W) of the confining layers of the LED when thin (<1000-Å) active regions are used. However, measured efficiencies decreased below 1% and lasing was no longer observed in devices with cavity thickness below 1000 Å.

B. EFFECT OF CAVITY THICKNESS ON FAR-FIELD PATTERN

The narrowing of the far-field pattern with thin (<1500-Å) active regions in edge-emitting LEDs has been established with AlGaAs devices [7]. A narrow far-field pattern means that the light is concentrated into a narrow angular spread and thus more power can be coupled into an optical fiber: >1% has been reported with AlGaAs devices. InGaAsP/InP edge-emitting LEDs with thin active regions were fabricated during the present contract with the hope of improving the coupling efficiency of 1.3-μm LEDs to fibers. Both LPE- and VPE-growth technologies were employed. LPE devices with cavity thicknesses of 1800, 1400, 900, 500 and 300 Å and VPE devices with 1100, 750 and 500-Å cavities were synthesized. Edge-emitting devices with 12-μm-wide contact stripes were fabricated in all cases. The far-field emission patterns perpendicular to the
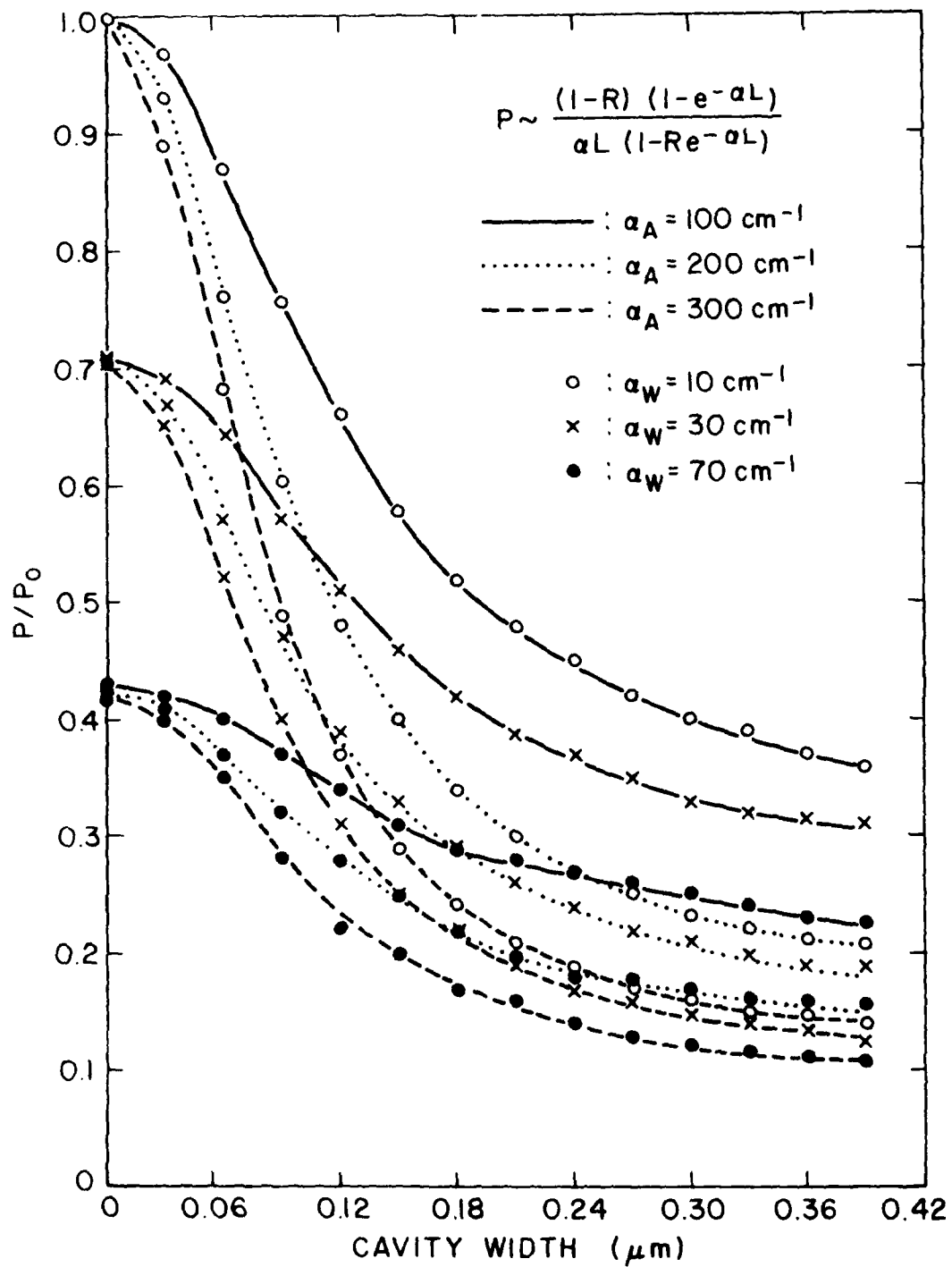
Figure 4. Calculated relative LED power output vs cavity thickness as a function of cavity (α_A) and waveguide (α_W) absorption coefficients.

8

Figure 5. Experimental setup for far-field pattern measurements.

junction plane were then measured to determine the extent of narrowing of the output light beam. The experimental setup for these measurements is shown in Fig 5. The far-field pattern was measured by rotating the device so that initially the p-side normal is colinear with the detector (0°) and finally the n-side normal is colinear (180°); 90° is the facet normal. Figures 6 to 11 show the measured far-field patterns for a number of these devices. Briefly, the results can be summarized as follows:

(1) Regardless of the cavity thickness, extra peaks always appear in the 90° to 150° angular range (n-side) which tend to broaden the patterns.

(2) If the half-widths of the far-field patterns are determined solely from the 0° to 90° emission (p-side), a distinct narrowing of the patterns occurs as the cavity thickness is reduced, which agrees well with predictions from waveguide theory. (See Table 2.)

(3) The net result of these two effects is that fiber-coupling efficiency was not significantly improved with thin-cavity devices; in

9

fact, highest coupling efficiencies were obtained from LEDs with cavity thicknesses in the range 1100 to 1700 Å.

Figure 6. Far-field pattern (perpendicular to junction) for an LPE 1.3-μm InGaAsP/InP LED with a 530-Å cavity.

Figure 7. Far-field pattern (perpendicular to junction) for LPE 1.3-μm InGaAsP/InP LED with a 530-Å cavity.

Figure 8. Far-field pattern (perpendicular to junction) for
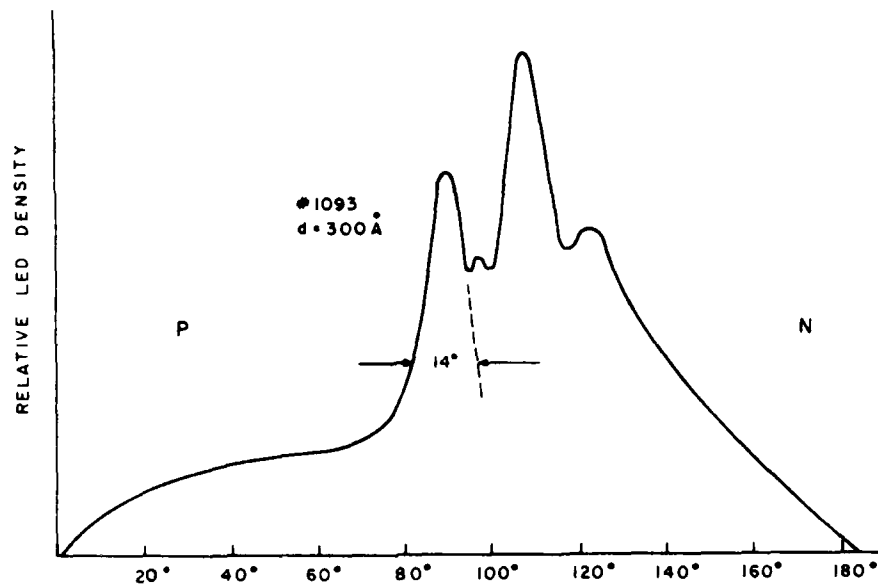LPE 1.3-μm InGaAsP/InP LED with a 750-Å cavity.

Figure 9. Far-field pattern (perpendicular to junction) for
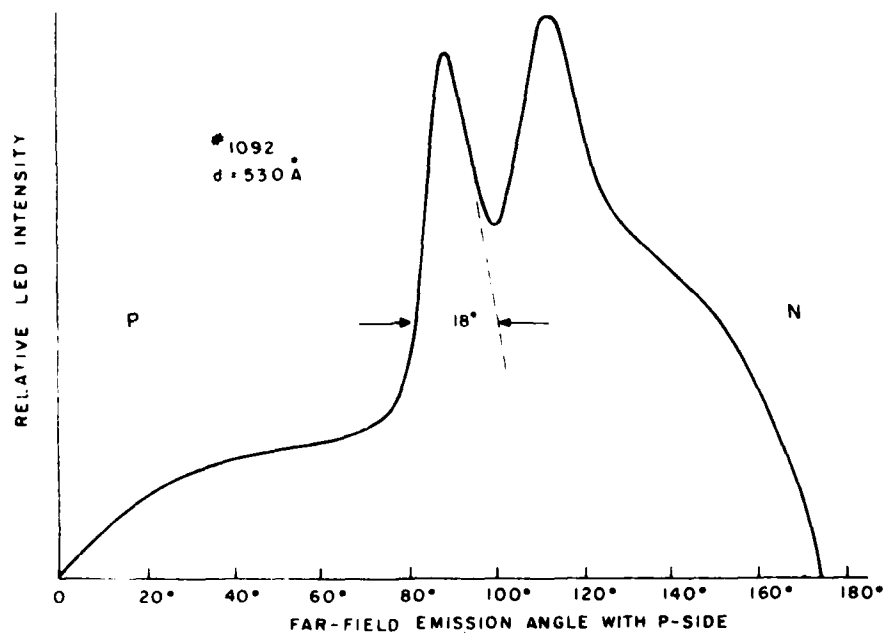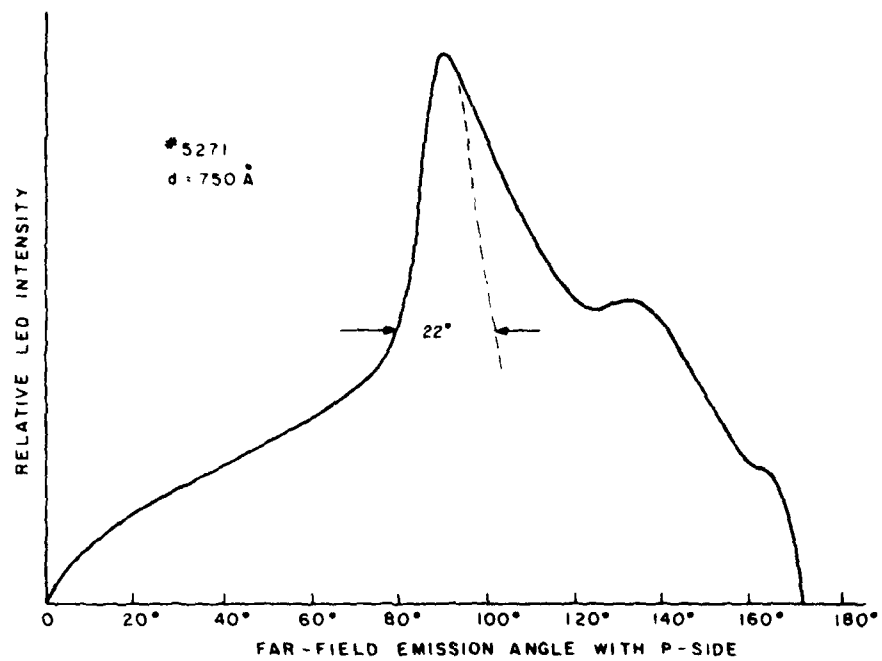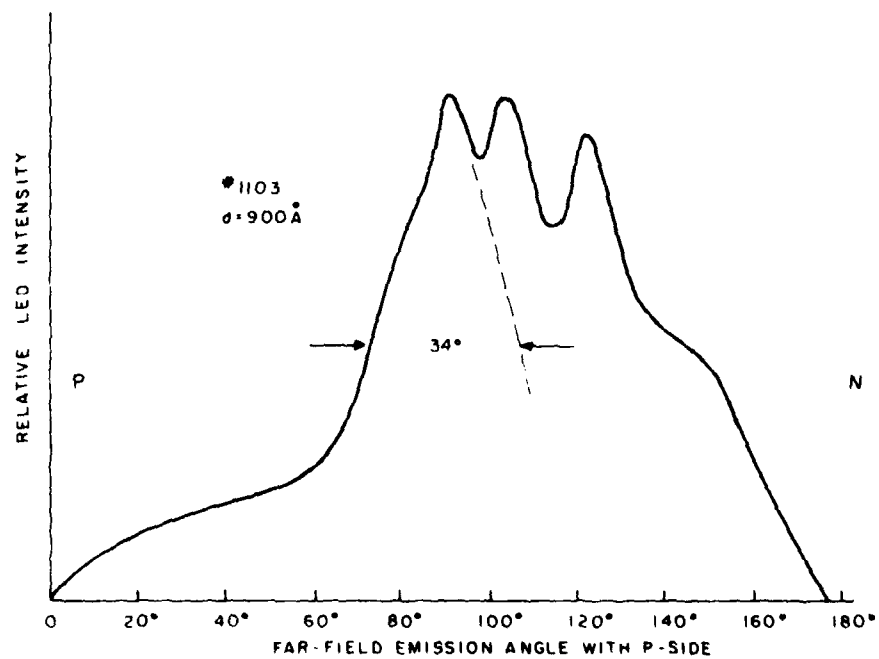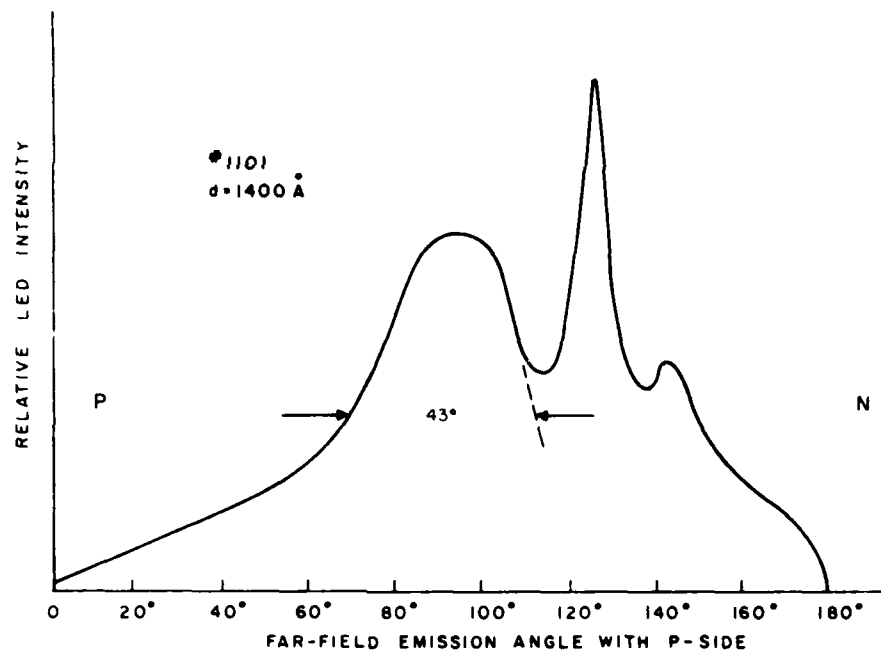LPE 1.3-μm InGaAsP/InP LED with a 900-Å cavity.

11

Figure 10. Far-field pattern (perpendicular to junction) for
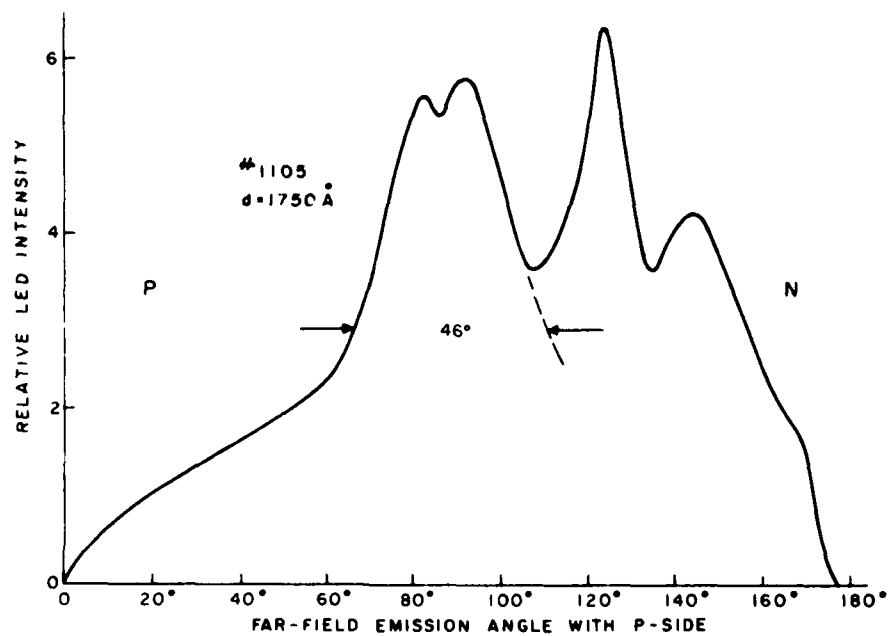LPE 1.3-μm InGaAsP/InP LED with a 1400-Å cavity.

Figure 11. Far-field pattern (perpendicular to junction) for
LPE 1.3-μm InGaAsP/InP LED with a 1750-Å cavity.

TABLE 2. FAR-FIELD HALF-WIDTHS ESTIMATED FROM THE 0°-to-90°
ANGULAR SPREAD

#	Cavity Thickness (Å)	Estimated Full-Width at Half-Power (degrees)	
		(Exp)	(Calc)
1093	300	14	11
1092	530	18	19
5271	750	22	25
1103	900	34	31
1101	1400	43	43
1105	1750	46	49

The half-width of the far-field pattern perpendicular to the junction can be estimated [7,8] from calculations made for guided radiation in devices with thin active regions. Figure 12 shows a plot (after Botez [8]) of half-width vs the ratio of cavity thickness (d) to wavelength (λ). The light is "trapped" both in the active layer as well as in the cavity formed by the active and confinement layers. It has been shown theoretically [9,10] and practically [10] that in the plane perpendicular to the junction the far-field pattern is composed of a middle lobe centered at 90°, corresponding to active-layer-guided light, and side lobes corresponding to confinement-layer-guided light. Therefore, it is quite reasonable to assume that the radiation lobe centered at 90° in Figs. 6-11 represents light guided by the active layer. Since almost no extra radiation is emitted on the p-side one can extrapolate the curves to estimate the beam width at half-power for the radiation emitted from the active layer. The agreement between experimental and calculated values (Table 2) is fairly good, considering the complexity of the far-field patterns. Figure 12 also contains the experimental points from which a refractive index is step (Δn) of 0.28 can be inferred. This value is in good agreement with values predicted for 1.3-μm InGaAsP/InP LEDs.

7. M. Ettenberg, H. Kressel, and J. P. Wittke, IEEE J. Quantum Electron. QE-12, 360 (1976).
8. D. Botez, RCA Rev. 39, 577 (1978).
9. Y. Seki, Jpn. J. Appl. Phys. 15, 327 (1976).
10. Y. Horikoshi, Y. Takanashi, and G. Iwane, Jpn. J. Appl. Phys. 15, 485 (1976).
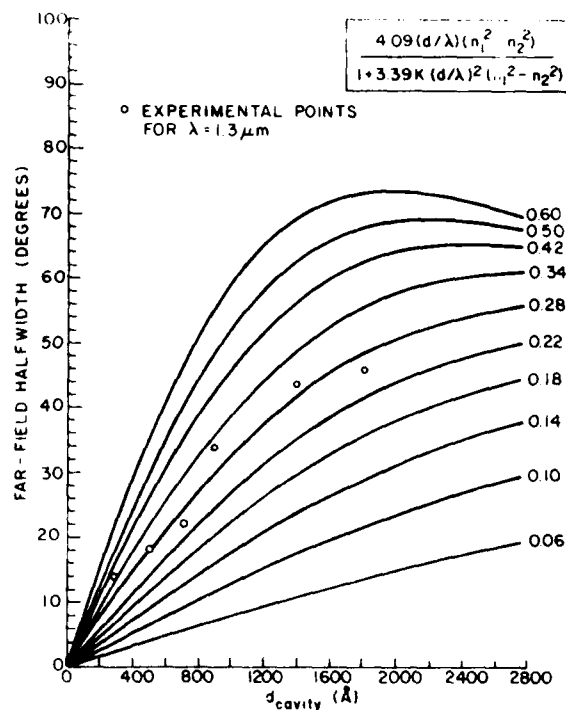
Figure 12. Calculated far-field pattern half-width (reference 8) for
guided radiation vs cavity thickness (d) divided by wave-
length (λ) as a function of heterojunction refractive
index step (Δn). Experimental points are from Table 2.

The origin of the extra radiation is still unclear but undoubtedly it is
related to fundamental differences between the AlGaAs and InGaAsP structures:
e.g., InGaAsP devices have a <u>transparent</u> substrate whereas AlGaAs devices have
an <u>absorbing</u> substrate. The possibility of extraneous reflections from the
top and bottom surfaces of the LED was checked by comparing far-field patterns
taken with TE, TM, and no filter. Results are shown in Fig. 13. Note that
the TE and TM components both have roughly the same magnitude. This indicates
that the extra peaks probably did not arise from reflections at either the top
or bottom of the chip since reflected light tends [11] to be polarized TE as
shown in Fig. 14 for a <u>laser</u>. Further discussions may be found in the next
section.

C. CONTROL OF InGaAsP LED FAR-FIELD PATTERNS WITH ABSORBING LAYERS

The reason for the lack of pronounced narrowing of the InGaAsP LED far-
field patterns with narrow cavities, as occurs in AlGaAs [7] for t < 1000 $\overset{\circ}{A}$,

11. H. Kressel and J. K. Butler, Semiconductor Lasers and Heterojunction LEDs,
(Academic Press, NY, 1977).

Figure 13. Perpendicular far-field patterns from an LED with no filter, a TE filter, and a TM filter which indicate that the light is not strongly polarized.
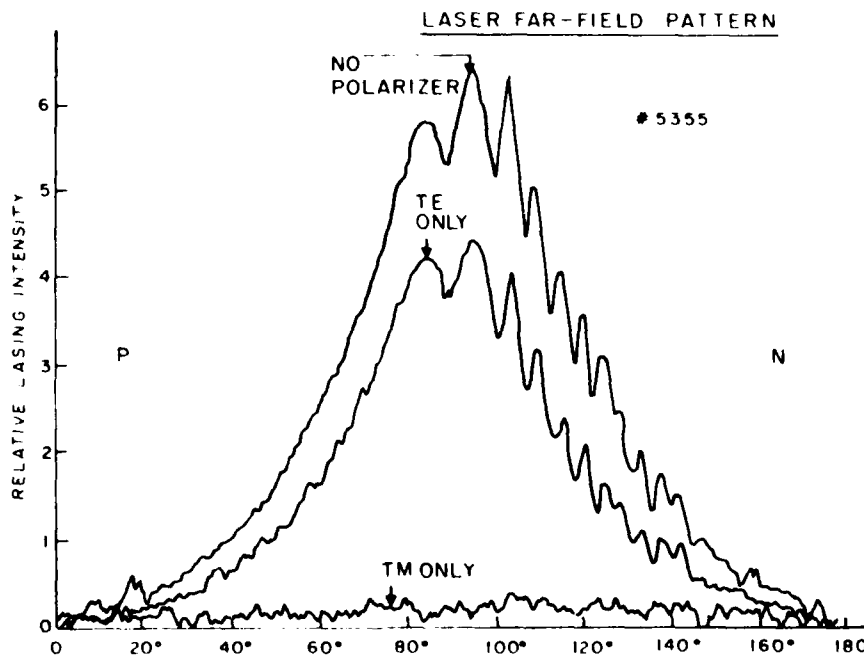
Figure 14. Far-field patterns from a laser with TE and TM filters which show that laser emission is strongly TE-polarized.
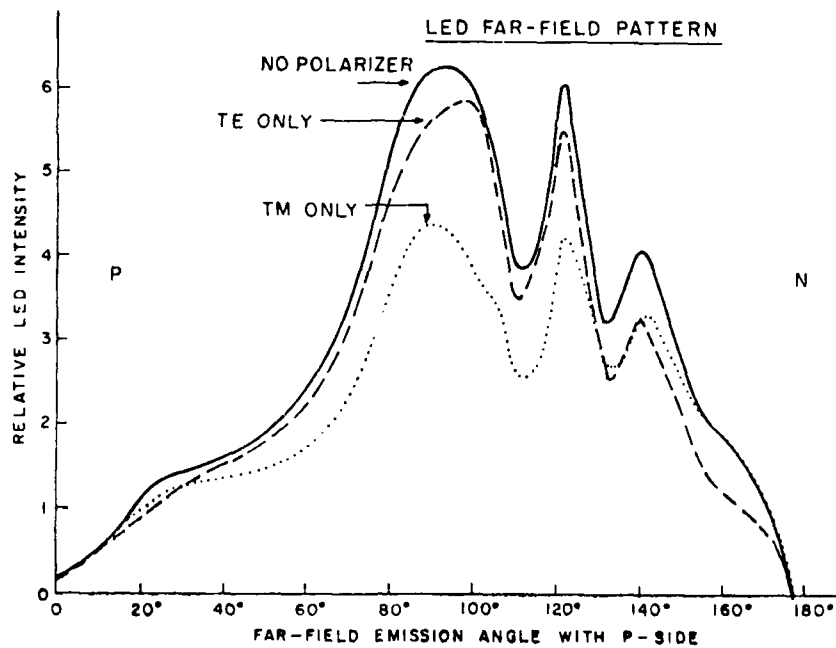
may be due to the difference in material properties encountered between the
two devices. Figures 15(a) and (b) show a comparison of the two structures.
Note that the AlGaAs device has both a substrate and a cap layer which is
highly absorbing, whereas the InGaAsP device has a completely transparent
substrate and a weakly absorbing cap layer. This difference could account for
(a) the lack of symmetry, and (b) lack of narrowing in the InGaAsP far-field
pattern, since any leakage of radiation from guided radiation along the cavity
would not be absorbed as is the case for AlGaAs.

(a) NORMAL AlGaAs   (b) NORMAL InGaAsP

(c) InGaAsP WITH ABSORBING CAP   (d) InGaAsP WITH ABSORBING
                                       CAP AND SUBSTRATE

(WIDTH OF LAYERS INDICATE RELATIVE ABSORPTION)
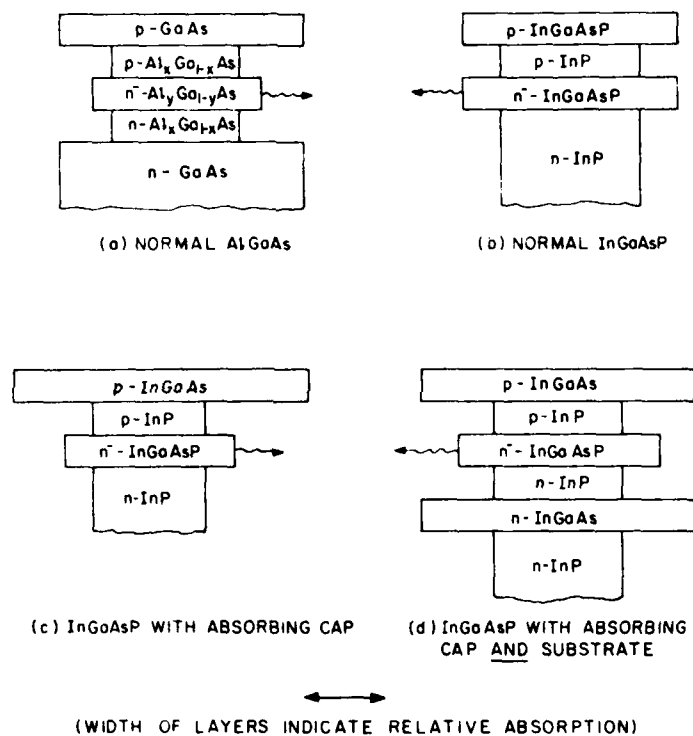
Figure 15. Sketch of various double-heterostructures used to
make LED devices.

The effect of an additional absorbing layer upon the far-field pattern of
InGaAsP LEDs is shown in Fig. 16. Figure 16(a) shows the far-field pattern for
a conventional InP/InGaAsP/InP LED structure [i.e., Fig. 15(c)] with an
1400-$\overset{\circ}{A}$ cavity. Note again that while some narrowing is observed on the p-side
of the junction, pronounced asymmetry is observed on the n-side in the form of
a second peak near 125°. Figure 16(b) shows a far-field pattern from an

WITHOUT ABSORBING CAP

#1101
d=1400 Å

(a)

WITH ABSORBING CAP
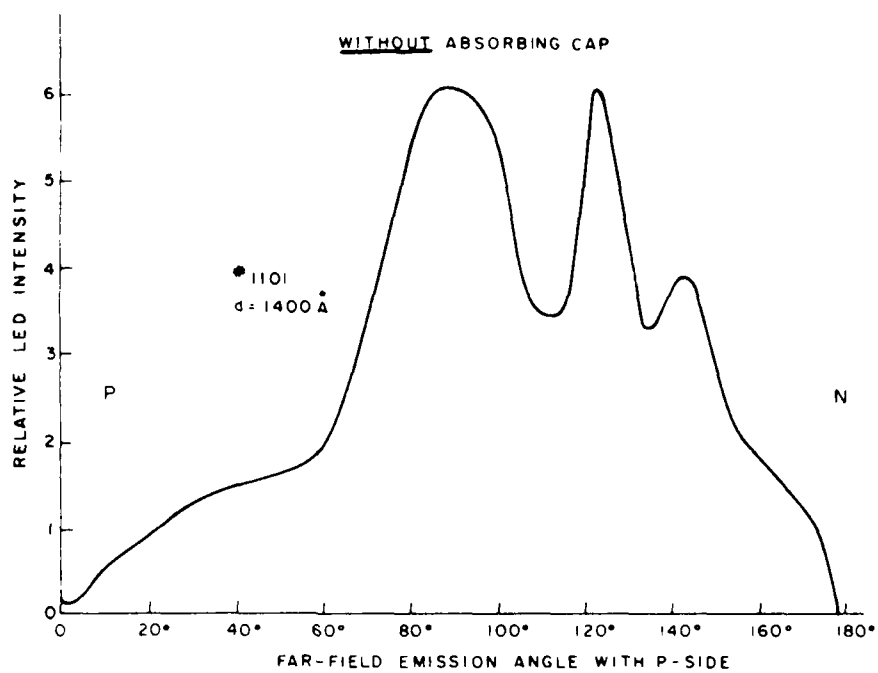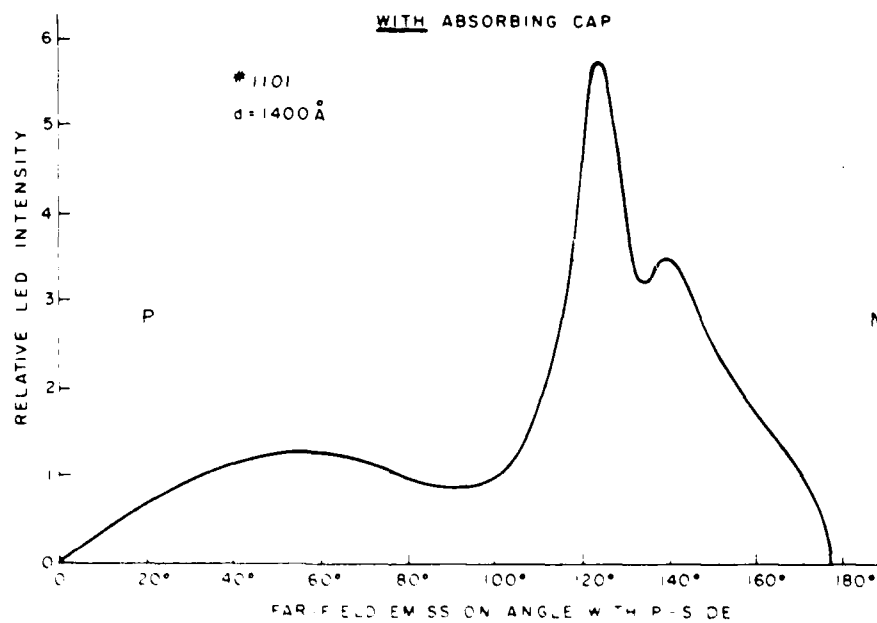
#1101
d=1400 Å

(b)

Figure 16. Perpendicular far-field patterns for a 1.3-μm InP/InGaAsP/InP LED with (b) and without (a) an absorbing InGaAs cap layer.

InGaAsP LED made from the same wafer (#1101) upon which a 2-μm highly absorb-
ing p-side InGaAs (λ = 1.7 μm) layer was vapor-deposited. Note that whereas the
main emission peak (near 90°) has been almost completely suppressed, the side
lobe, near 125°, is still evident. This strongly suggests that (a) the ab-
sorbing layer is too close to the cavity, and thus tends to quench the main
beam, and (b) the secondary peak originates as radiation which leaks out the
nonabsorbing substrate side of the device.

An attempt was also made to vapor-grow a quaternary LED which would be
similar to an AlGaAs device, i.e., with two highly absorbing layers symmet-
rically arranged about the cavity as shown in Fig. 15(d). This structure had
a cavity thickness of 0.18 μm, InP thicknesses of 1 μm, and InGaAs absorbing
layer thicknesses of 0.4 μm. Figure 17 shows the far-field pattern obtained
from such a device. Some leakage is still evident near the 125° region,
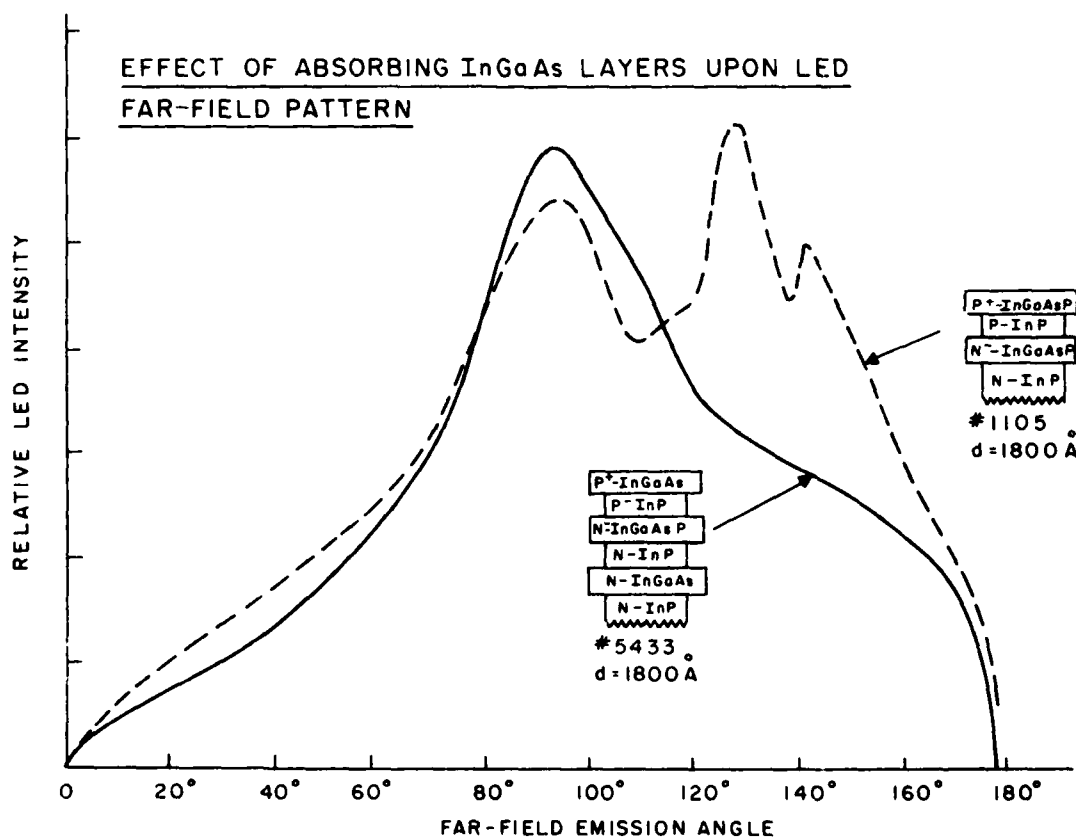perhaps due to the thinness (0.4 μm) of the underlying absorbing layer.

Figure 17. Far-field pattern from a 1.3-μm InP/InGaAsP/InP LED with
symmetric underlying (substrate) and overlying (cap)
InGaAs absorbing layers.

18

Although the main beam at 90° is the predominant one here, no pronounced narrowing is observed. However, the half-width (45°) as estimated on the 0° to 90° side of the pattern is consistent with that calculated for an 1800-Å cavity. It should also be noted that the LED efficiency of this device was poor ($\sim$0.2%), again probably due to the closeness of the absorbing layers to the LED cavity.

Although, the simple type of LED far-field pattern narrowing as is observed in AlGaAs devices was not observed in InGaAsP devices, the following features were evident.

1. Guided radiation is observed in InGaAsP LEDs with cavity thickness $\leq$1000 Å.

2. Multiple beams are observed in these structures due to radiation leakage from the cavity and lack of an absorbing substrate.

3. These extraneous beams can be controlled and/or suppressed by the addition of highly absorbing layers, however, there is a consequent decrease in external efficiency.

Further research with InGaAsP/InP LED structures of the type shown in Fig. 15(d) may well demonstrate the ability to achieve the same narrow far-field patterns (and, thus, improved coupling efficiency) as is observed with AlGaAs LEDs.

As mentioned previously, side lobes in the transverse far-field pattern can correspond to radiation guided by the confinement layers. However, even if the cavity is highly asymmetrical these lobes should occur symmetrically with respect to the 0° axis. Asymmetrical far-fields will be observed only when a radiation-loss mechanism is at work. Therefore, we suspect that the side-lobes shown in Figs. 6-11 correspond to confinement-layer-guided light that is subject to absorption and/or leaked out into the quaternary "cap" layer or the metallic stripe contact. Our structures are particularly prone to such effects since there is no boundary on the n-side and thus the radiation that escapes the active layer will be guided only between the active layer and the cap layer; that is leakage to and absorption into the cap layer and the metallic stripe contact are quite favored.

19

III. TEMPERATURE DEPENDENCE OF LED EMISSION

The temperature dependence of LED power efficiency, emission wavelength, and spectral half-width have been measured for both VPE and LPE edge-emitting LEDs over the temperature range of 22° to 70°C. The results are shown in Figs. 18-20. These data show that the LED efficiency drops with temperature, about 30% between 20° to 70°C, as is found with GaAs LEDs [11]. InGaAsP devices [12,13] seem to exhibit high-temperature dependencies; InGaAsP lasing thresholds obey an exponential temperature dependence of $I_{TH} \sim \exp(\Delta T/T_o)$ where $40 < T_o < 70°C$. GaAs devices, on the other hand, exhibit T_o values in the range 140° to 190°C (and sometimes higher). High-temperature dependence has also been found for InGaAsP carrier lifetimes. The pronounced temperature dependence of InGaAsP device properties has been attributed to the presence of both non-radiative recombination, via impurity centers, and band-to-band Auger recombination. Although indirect evidence is accumulating for these effects, no single, conclusive cause for the high-temperature dependence of InGaAsP has been found.

Recalling that the output power (P) of an LED varies [4] as

$$P/P_o \sim \eta_{sp} \ (1 - e^{-\alpha L})/\alpha L$$

then the decrease in P with temperature could be due to increases in absorption (α) or to decreases in the internal spontaneous efficiency (η_{sp}). Substantial changes in the value of α (i.e., 100 to 200 cm^{-1}) with temperature would not cause the observed behavior. This is borne out experimentally by the curves in Fig. 21 which show similar temperature dependence of LED efficiency for diodes of 100- and 200-µm length (L). Therefore, the decrease in LED efficiency with temperature (T) must be due to a decrease in η_{sp}. This variation of η_{sp} with T could possibly be due to the presence of nonradiative recombination centers which are thermally activated. A plot of η_{sp} (relative) vs temperature is shown in Fig. 22 for both the LPE and VPE LEDs. Assuming that the nonradiative recombination varies as $\exp(-E_A/kT)$, an activation energy of 0.1 to 0.2 eV can be deduced. Data for InGaAsP devices from other references [10,11] which show a similar temperature dependence of efficiency are also shown in Fig. 22.

12. G. B. Thompson and G. D. Henshall, Electron. Lett. 16, 43 (1980).
13. Y. Horikoshi and Y. Furukawa, Jpn. J. Appl. Phys. 18, 809 (1979).
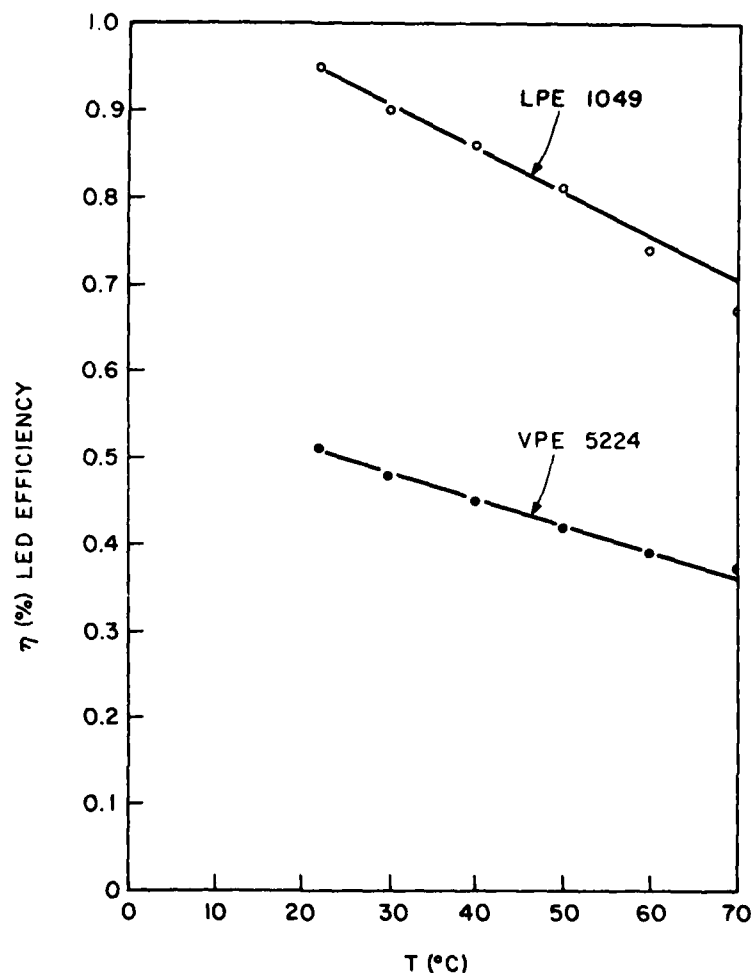
Figure 18. LED power efficiency vs temperature for both VPE
and LPE edge-emitting LEDs.

Activation energies of 0.1 to 0.3 eV were proposed. The claim for an "acti-
vation energy" is only a phenomenological model which does not identify the
type of center or impurity responsible for the thermal behavior. Further
fundamental materials work on InGaAsP is needed to elucidate the cause of this
high-temperature dependence of device properties which seems to plague the
alloy system over its entire lattice-matched range (to InP: 1.0 to 1.7 μm).

The dependence of LED emission wavelength and spectral half-width are
shown in Figs. 19 and 20 for both VPE and LPE devices. The VPE device exhibits
a wavelength shift of 5.8 Å/°C (0.44 meV/°C) and a spectral halfwidth change of
650 to 950 Å over the temperature range of 22° to 70°C. The LPE device shows

21

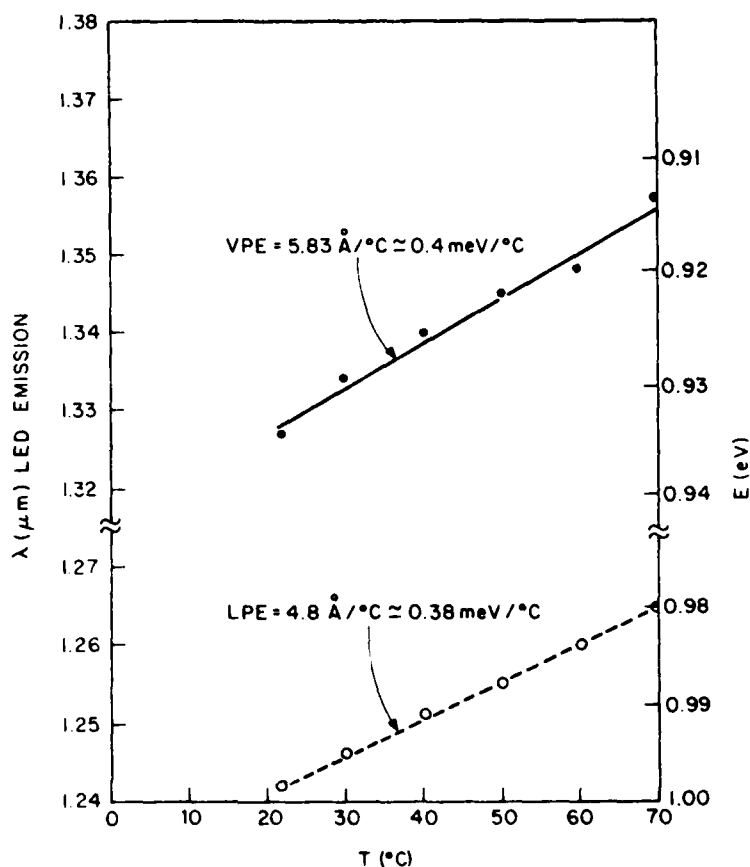Figure 19. Emission wavelength vs temperature for both VPE
and LPE edge-emitting LEDs.

changes ot 4.8 Å/°C (0.38 meV/°C) and 1170 to 1250-Å half-width shift over the
same temperature range. The wavelength shift with temperature is consistent
with other reports in the literature for InGaAsP devices (4 to 6 Å/°C) and is
due to the decrease in bandgap with temperature. The narrow VPE spectral
half-width is due both to the low background doping density (1×10^{16} cm^{-3})
of the cavity together with absorption effects of the edge-emitting structure.
The wider LPE spectral width is most likely due to higher cavity doping levels
or doping compensation in the active region since the geometries of the two
structures are identical. It is generally mo.e difficult to maintain low
doping densities in multibin (multilayer) LPE growth due to cross contamination
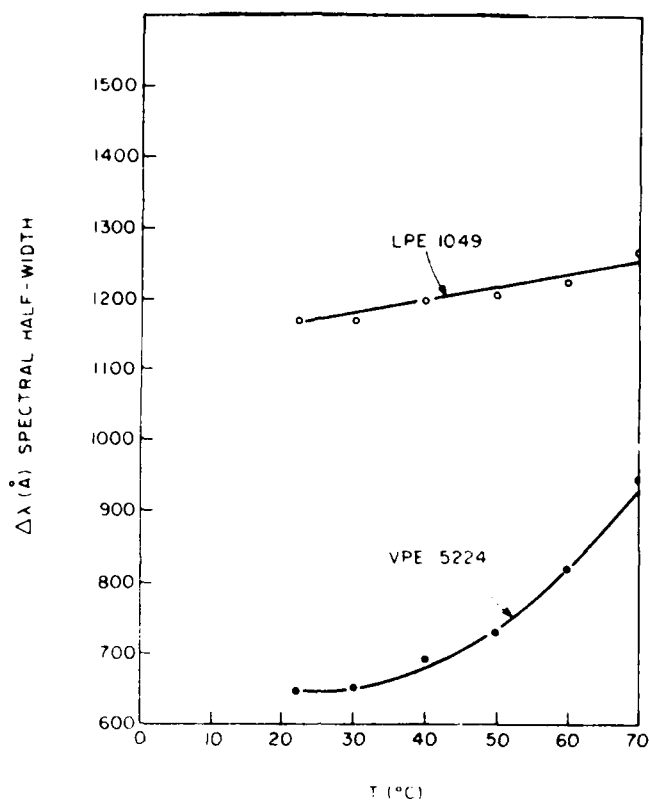from bin to bin.

22

Figure 20. Spectral half-width vs temperature for both VPE
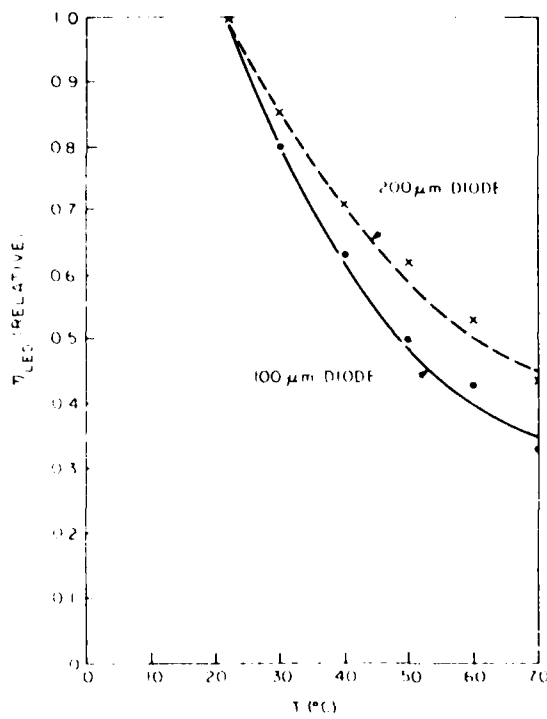and LPE edge-emitting LEDs.

Figure 21. LED efficiency vs temperature for 100-μm- and 200-μm-long
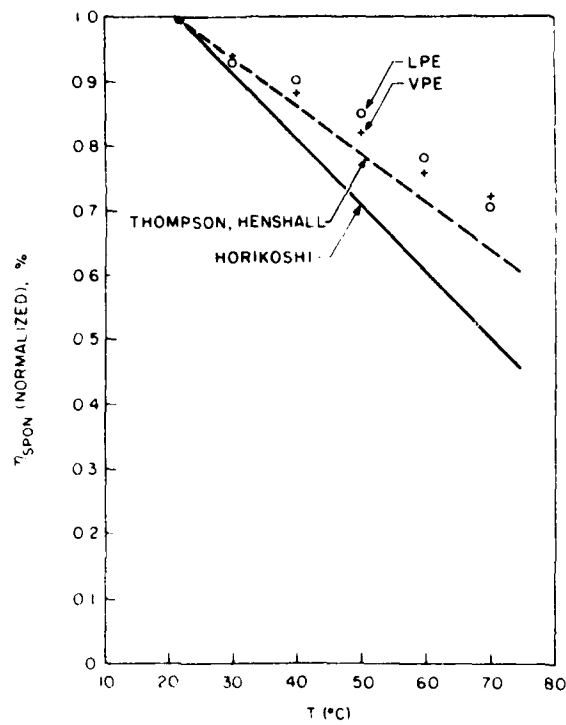VPE edge-emitting LEDs.

23

Figure 22. Relative LED efficiency vs temperature for VPE and
LPE edge-emitting LEDs. Data from references 2 and 3
are also included.

IV. COUPLING RESULTS

A. COUPLING OF VPE AND LPE EDGE-EMITTING LEDs TO 50- AND 100-μm FIBERS

The effect of fiber diameter on coupling efficiency for VPE and LPE LEDs was determined by coupling the light from the two devices into 50- and 100-μm core diam, graded index fibers with NA > 0.21. Results are shown in Figs. 23 and 24. The fiber coupling efficiency more than doubles (2.0 to 2.6X) when using the 100-μm diam fiber. However, harmonic distortion and dispersion increase with fiber diameter and can sometimes cancel out the benefit of the increased coupled power. Optimum fiber parameters must always be determined by the speed, power, and frequency requirements.

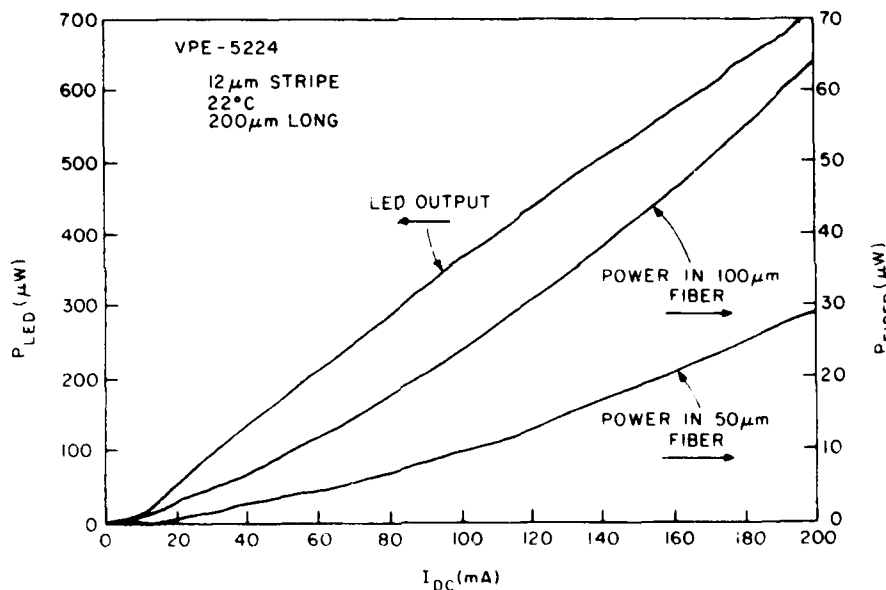Figure 23. Power coupled into 50- and 100-μm fibers vs drive current for a VPE edge-emitting LED.

B. HIGH COUPLING EFFICIENCIES FROM NARROW-STRIPE 1.3-μm VPE AND LPE InGaAsP/InP LEDs

Very high coupling efficiencies have been measured for both LPE and VPE InGaAsP/InP 1.3-μm edge-emitting LEDs. Coupling efficiencies as high as 13.4% have been measured in VPE LEDs. These increases are attributed to a narrow
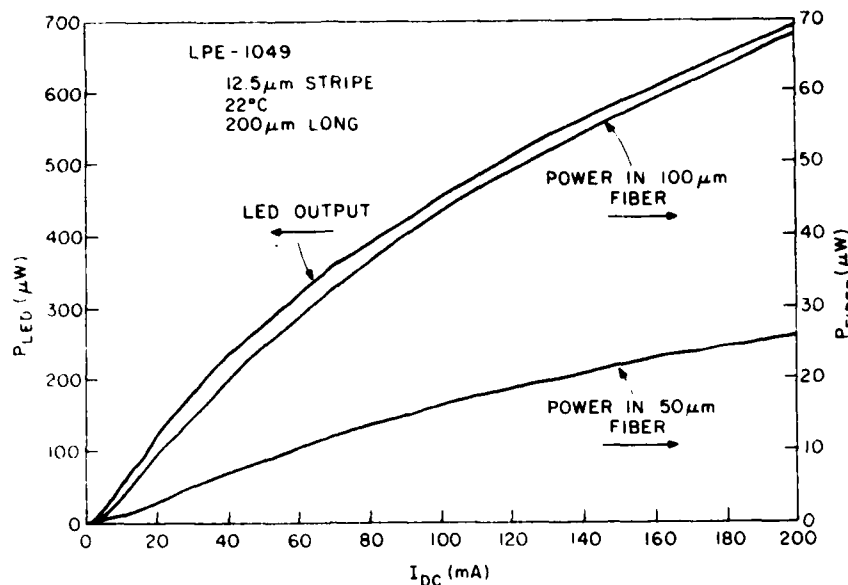
Figure 24.   Power coupled into 50- and 100-μm fibers vs drive
current for an LPE edge-emitting LED.

Figures 25, 26 and 27 highlight the coupling results for both LPE and VPE
LEDs with the 12-μm contact stripe. Figure 25 contains a plot of highest
coupled power vs drive current for a VPE LED. Note that 135 μW were coupled
into a 55-μm core 0.25-NA graded-index fiber. This corresponds to a coupling
efficiency of 13.4%. More typical values of coupled power obtained from both
VPE and LPE are shown in Figs. 26 and 27. Typical measured coupling efficiencies
into lensed (balled) fibers from both devices were 8% (coupling efficiency
here is defined as the ratio of power launched into the fiber to power out of
the LED). All results quoted here are for mode-stripped fibers whereby any
power coupled into the fiber cladding is eliminated. Also shown in the
figures are the power coupled into cleaved fibers. In both cases more power
was coupled into the lensed (balled) fiber rather than the cleaved fiber. A
photograph of the two types of fiber ends is shown in Fig. 28.   For the VPE
device the coupling efficiency dropped from 8% to 6% with cleaved fibers,
whereas the efficiency with the LPE device dropped markedly from 8% to 2.5%.
The reason for the large drop with the LPE device is not understood. However,
it may have to do with the large amount of current spreading which occurred
under the contact stripe which creates a larger effective source size.
Figure 29 shows comparisons of the near-field patterns of both the VPE and
LPE devices which had 12-μm contact stripes.   The VPE device exhibits good

26
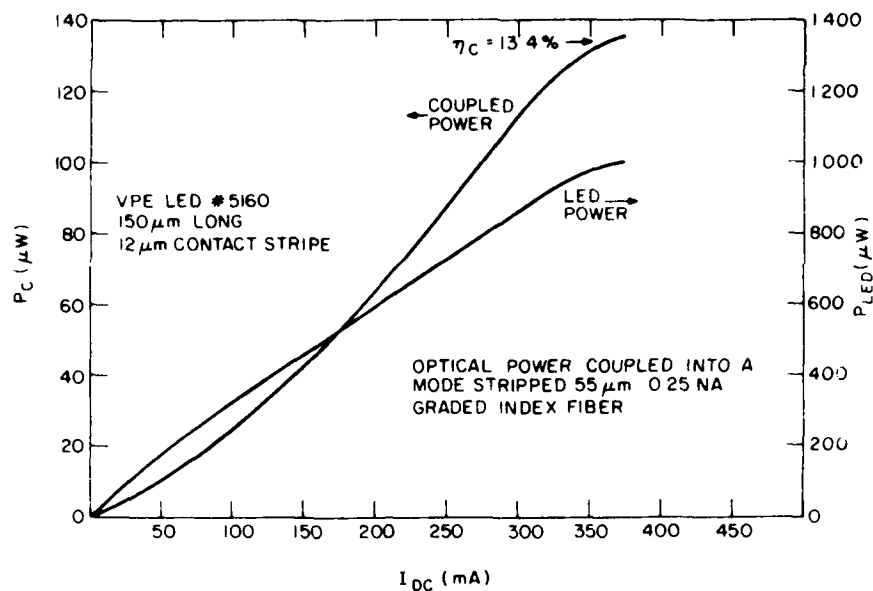
Figure 25. Highest coupled optical power in a mode-stripped
fiber vs LED drive current for a VPE LED.
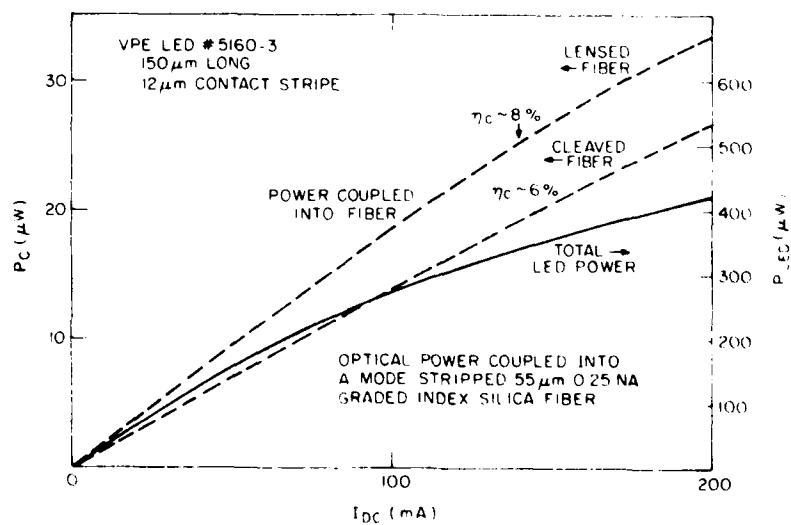
Figure 26. Typical coupled optical power in a mode-stripped
fiber vs LED drive current for a VPE LED.

27
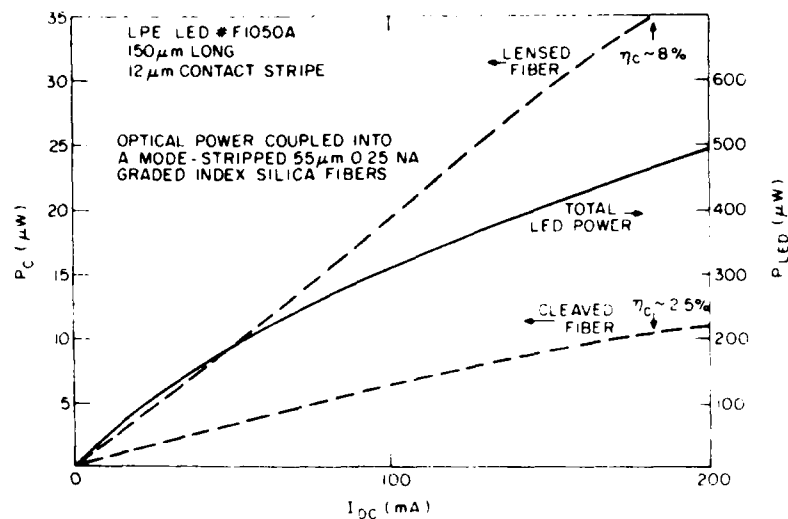
Figure 27. Typical coupled optical power in a mode-stripped
fiber vs LED drive current for an LPE LED.

it may have to do with the large amount of current spreading that occurred
under the contact stripe, which creates a larger effective source size.
Figure 29 shows comparisons of the near-field patterns of both the VPE and
LPE devices which had 12-μm contact stripes. The VPE device exhibits good
current confinement (as judged by the light pattern) whereas the LPE device
exhibits considerably more spreading away from the contact. Spectra for the
two devices are shown in Fig. 30. The narrow spectral widths (620 and 640 Å)
are typical for edge-emitting devices and together with high-coupling effi-
ciencies represent their major advantage when employed as a light source for
fiber optical communications.
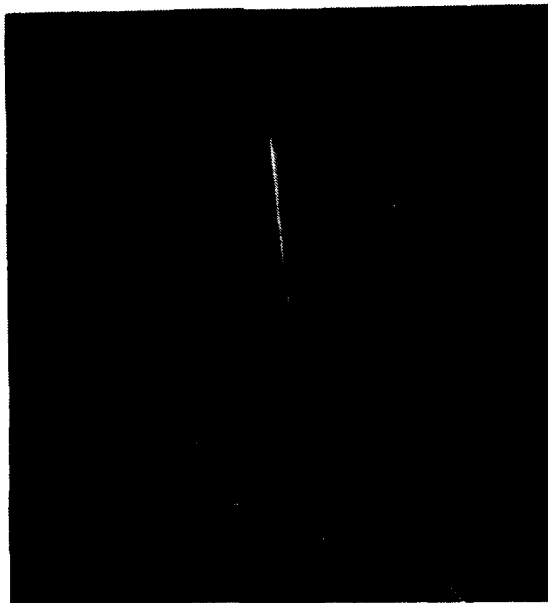
LENSED FIBER

CLEAVED FIBER

$100\mu m$

Figure 28. Optical photograph of cleaved and lensed (balled) fiber ends.

29

NEAR-FIELD PHOTOGRAPHS OF
1.3μm InGaAsP/InP LEDS

$10\mu m$

VPE 5160-3   LPE F 1050A-3
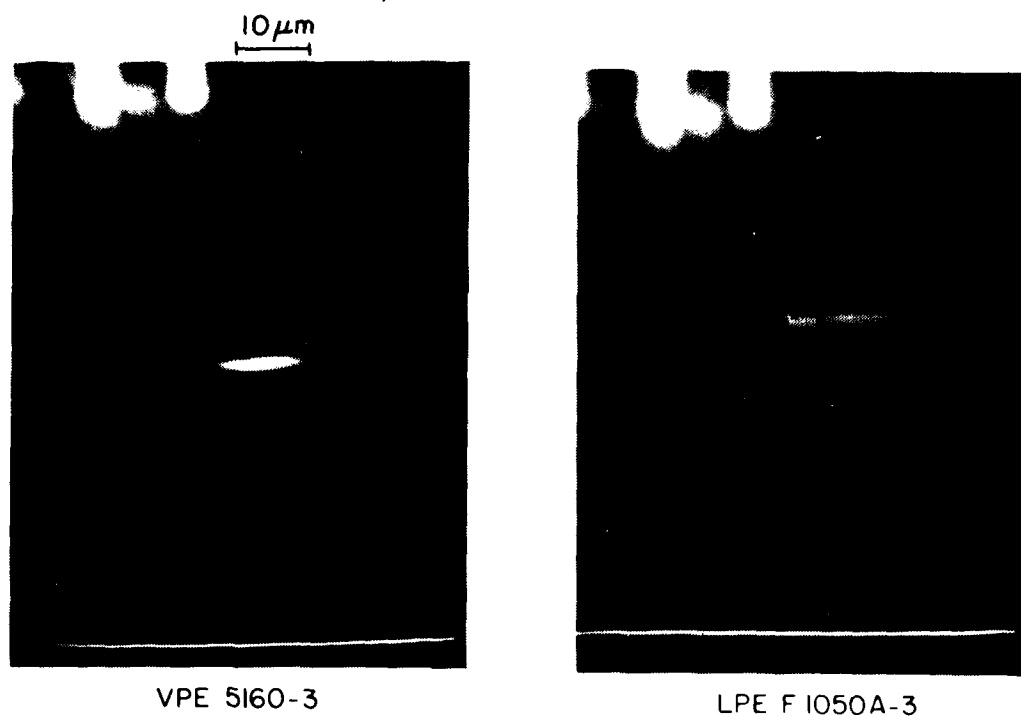
Figure 29.   Photographs of near-field patterns of VPE and LPE
with 12 contact stripes.

$\Delta\lambda = 640\mathring{A}$
$\Delta h\upsilon = 52.5 meV$

$\Delta\lambda = 620\mathring{A}$
$\Delta h\upsilon = 46 meV$

1.14 1.16 1.18 1.20 1.22 1.24 1.26 1.28 1.30 1.32   1.22 1.24 1.26 1.28 1.30 1.32 1.34 1.36 1.38 1.40

VPE 5160-3   LPE F 1050A 3
22 °C   22 °C
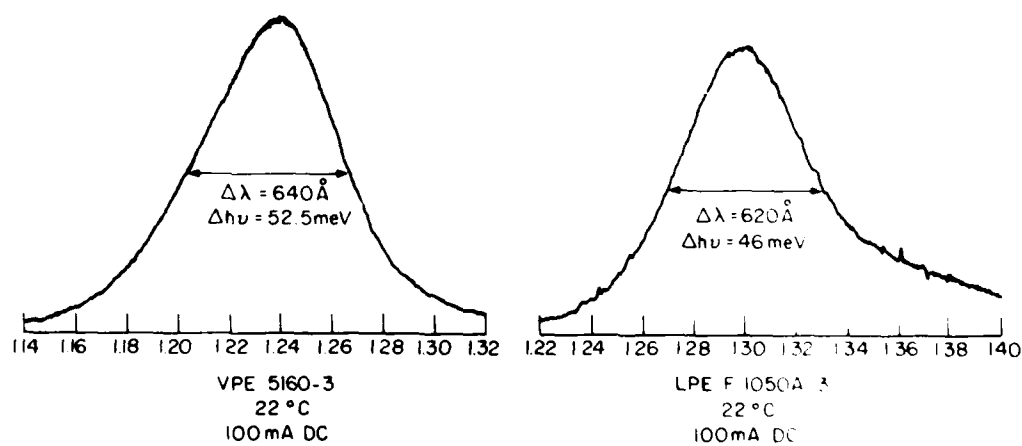100 mA DC   100 mA DC

Figure 30.   Optical spectra from VPE and LPE LEDs.

V. INDEPENDENT CHARACTERIZATION OF RCA EDGE-EMITTING LEDs

An RCA 1.3-µm InGaAsP/InP edge-emitting LED has been extensively characterized by an Italian group at the CENTRO STUDI E LABORATORI TELECOMUNICAZIONI S.P.A. GRUPPO STET in Turin, Italy, headed by Federico Tosco. Their results are summarized below. Although the coupled power efficiency (3%) seems low, complete details of the coupling procedures were not available. However, the 3-dB frequency response (250 MHz) and pulse risetime (500 ps) are particularly noteworthy.

A. INDEPENDENT CHARACTERIZATION OF InGaAsP/InP LED RCA 5221

The InGaAsP/InP double-heterostructure LED marked 5221 was tested for the following main characteristics:

Total Emitted Power Per Facet

The LED was butt-coupled to a Ge detector (Judson J16) with 0.5-mm active area diameter, previously calibrated at the emission wavelength of the LED.

Power Coupled into Fiber

The power coupled into a graded-index optical fiber (62.5-µm core diam, 0.15-numerical aperture) was measured; a mode stripper was used to avoid cladding mode effects. The Ge detector was the same as above.

Peak Wavelength and Spectral Width (FWHM)

These tests were carried out with a grating monochromator; a Ge APD (Optitron Ga-1) was employed as a detector. This system had a resolution of about 0.1 nm, as required by the modal pattern of the source.

Frequency Response

The source was sinusoidally modulated, detected by a Ge APD (Optitron Ga-1) which had about a 120-ps risetime with the output measured by a vector voltmeter. A small modulating signal was used (10 mA peak to peak).

Near Field Measurements

A near-field measurement was carried out in the plane parallel to the junction, scanning a magnified image of the source with a 100-µm square size Ge photo-detector.

Radiance

Owing to laser-like beam pattern characteristics of the examined device a precise evaluation of the radiance was difficult. We measured values on the order of $10^3 W/sr.cm^2$.

B. RESULTS

RCA 5221

- Total emitted power per facet @ 200 mA   0.9 mW
- Power coupled into fiber @ 200 mA
  (graded index optical fiber core = 62.5 µm, NA = 0.15)   25 µW
- Peak wavelength @ 200 mA, T = 25°C   1315 nm
- Spectral width (FWHM) @ 200 mA, T = 25°C   41 nm
- Frequency response (3-dB bandwidth)   250 MHz
- Pulse response (risetime)   500 ps
- Forward voltage @ 200 mA   1.6 V

VI. SPEED CHARACTERISTICS

A. AC MODULATION CHARACTERISTICS

The ac frequency-response characteristics of both VPE- and LPE-grown LEDs were measured by applying ac modulation and dc bias current to the devices. This was accomplished with a passive network that matched the impedance to that of a 50-Ω transmission line. The optical response was measured with a Ge avalanche photodiode and a sampling oscilloscope.

Figure 31 contains a plot of relative output vs modulation frequency for a VPE 1.3-μm LED using a bias of 200 mA and a peak-to-peak modulation current of 60 mA. The response dropped down by a factor of 2 (3 dB) at 200 MHz which is a significantly high value for an LED. A number of other devices (including LPE-grown units) had 3-dB points in the range of 100 to 200 MHz.
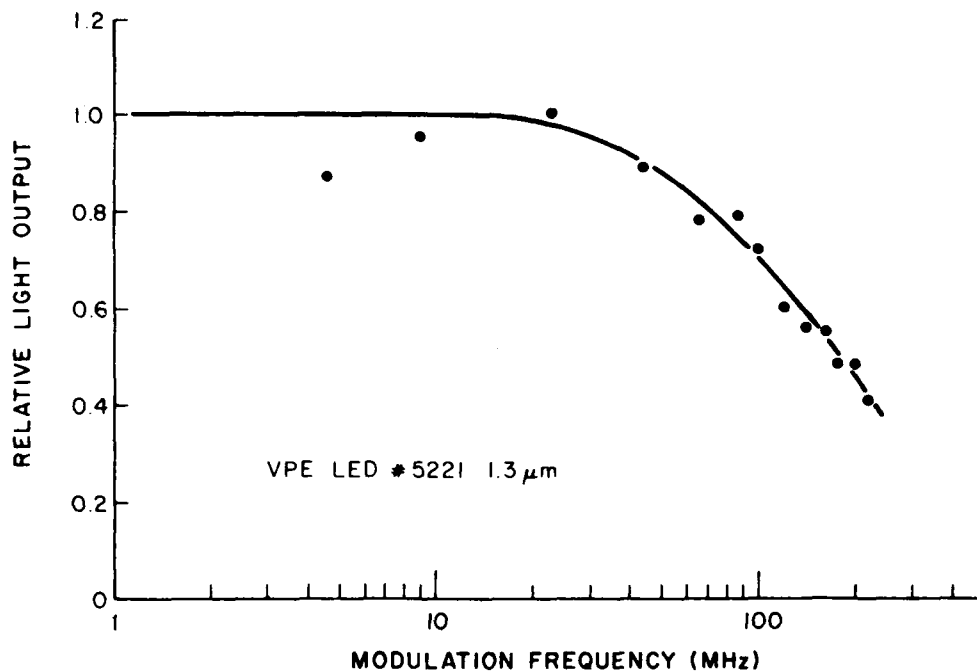
Figure 31. Relative LED power output vs ac modulation frequency for a 1.3-μm InGaAsP edge-emitting LED.

These results demonstrate yet another advantage of the edge-emitting narrow contact stripe LED geometry and show that these devices might be used in a number of applications where lasers are normally employed.

B. PULSE REPONSE

Improved pulse response has also resulted from the use of the narrow-stripe edge-emitting LED geometry. Figures 32 and 33 compare the fastest measured rise and fall time as a function of dc bias for both VPE and LPE LEDs. Note that the LPE device had a fall time and rise time of 2.4 and 2.0 ns, whereas the VPE device measured 3.4 and 2.4 ns. Typical values were in the range of 2 to 5 ns. Reducing the cavity thickness below 1500 Å did not significantly improve the pulse response as discussed in the next section.
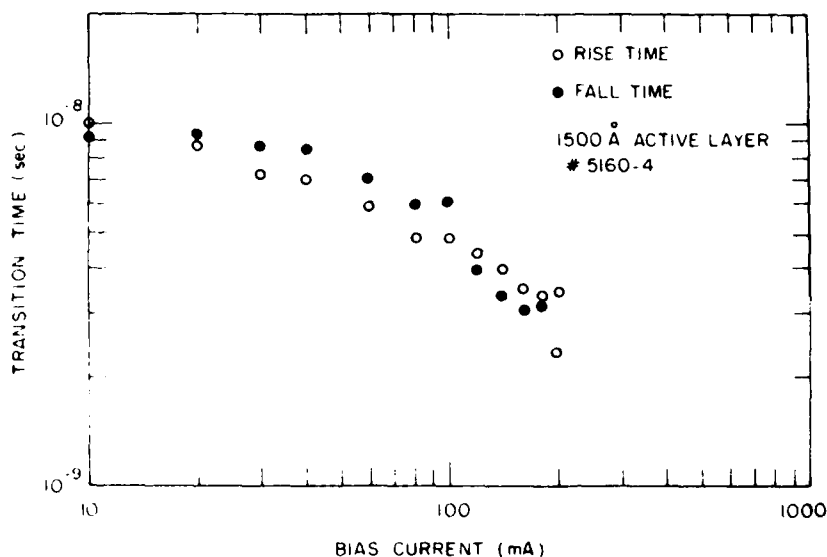

Figure 32. Rise and fall time (pulse response) vs drive
current for a VPE 1.3-μm InGaAsP LED

C. EFFECT OF CAVITY THICKNESS ON DEVICE SPEED AND POWER-BANDWIDTH PRODUCT

As previously mentioned, LED pulse response time decreased with increasing dc bias but did not appear to decrease as the cavity thickness was reduced below 1500 Å. Figure 34 contains a plot of rise and fall time vs dc bias for an LPE LED with a 300-Å cavity thickness which also demonstrates this behavior.
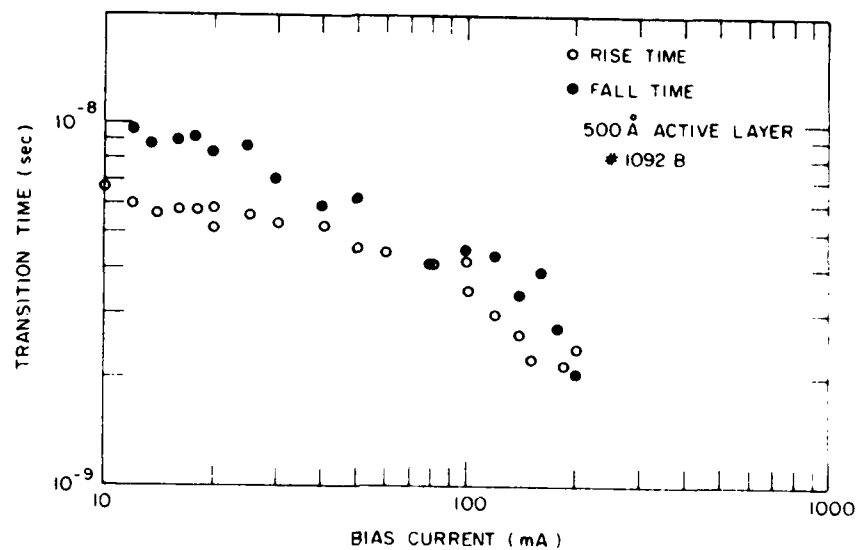
Figure 33. Rise and falltime (pulse response) vs drive
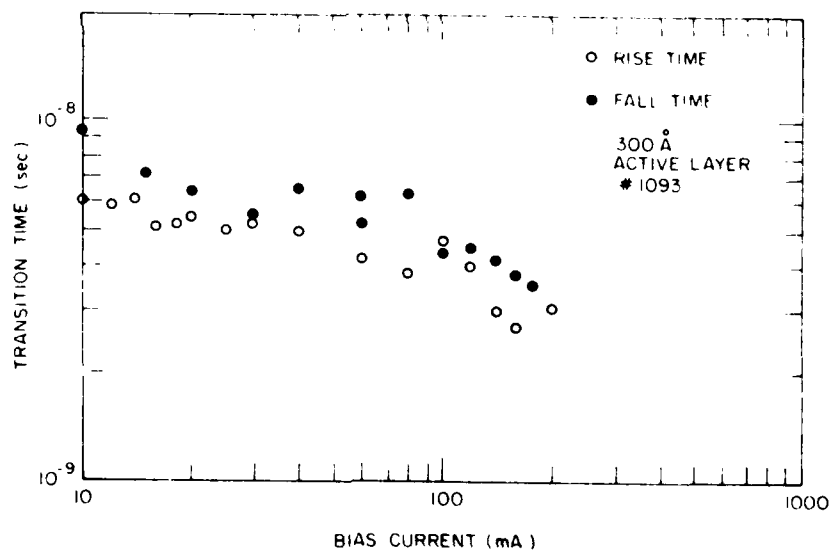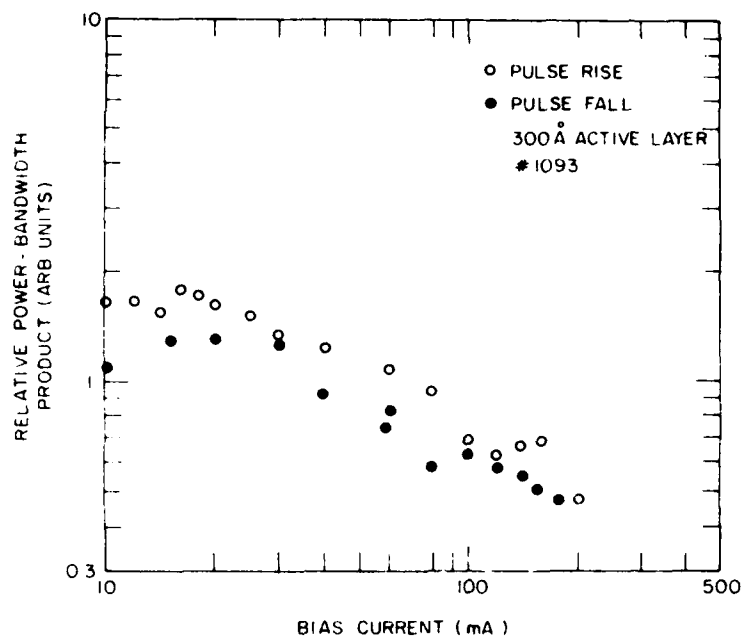current for an LPE 1.3-μm InGaAsP LED.


Figure 34. Rise and falltime (pulse response) vs drive
current for an LPE 1.3-μm InGaAsP LED with a
300-Å cavity.

35

However, the relative power-bandwidth product vs drive current did appear to vary with cavity thickness. Figure 35 contains plots of this data for LEDs with 300-, 500-, and 1500-$\mathring{A}$ cavities. The decrease in product with drive current (with thin cavities) is probably due to an earlier saturation with drive of the power output of very thin cavity devices which have lesser recombination volumes.

The observation on response time reported here can be interpreted in terms of physical processes within the active cavity. We have seen that reducing the cavity thickness has no substantial effect on the response time. This implies that the transit time of carriers in the cavity does not limit the response times. The response time decreased with increasing bias current, suggesting that nonlinear carrier recombination processes dominate. For the thick active layer devices we find the output increasing as the response time falls, giving an increasing power-bandwidth product with increasing bias current. This is consistent with bimolecular recombination processes. The thin active layer devices show an optical output saturation at high currents. This may be the result of higher carrier densities in the thin layers causing higher over recombination processes such as Auger processes.
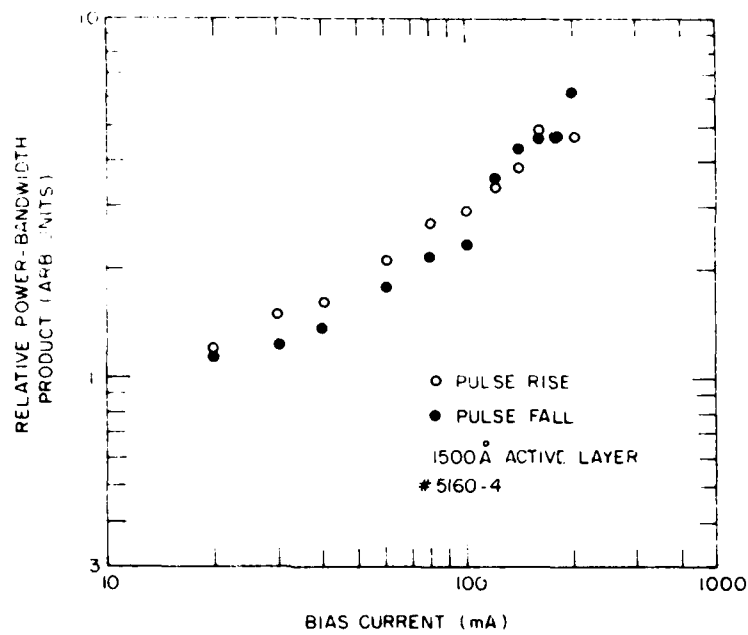
(a)
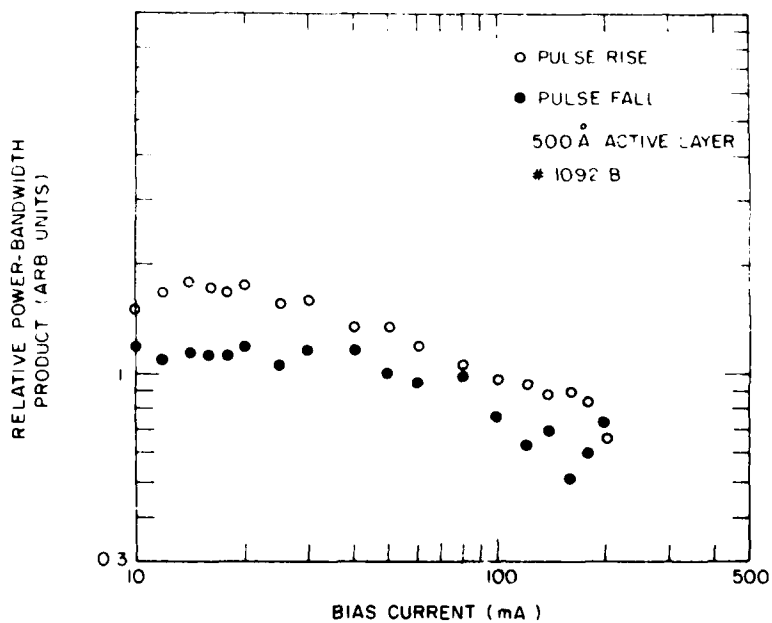
(b)

Figure 35.   Power-bandwidth product vs drive current for LPE 1.3-μm
InGaAsP LEDs with (a) 300-Å, (b) 500-Å, and (c) 1500-Å
cavities.

(c)

Figure 35. Power-bandwidth product vs drive current for LPE 1.3-μm InGaAsP LEDs with (a) 300-Å, (b) 500-Å, and (c) 1500-Å cavities.

38

VII. LED RELIABILITY

The reliability of InGaAsP edge-emitting LED structures has been evaluated under a past government contract (U.S. Army Contract No. DAAB07-77-C-2173-DARPA) as well as an ongoing one (U.S. Navy Contract No. N41756-79C-2858). Over 14,000 h of undegraded operation at 70°C has been observed with a set of VPE 1.3-µm InGaAsP/InP LEDs. A group of LPE devices has been operating for over 4000 h at 90°C without degradation. Thus, the reliability of InGaAsP/InP 1.3-µm LEDs would appear to be very high.

A recent development has been even more encouraging. Most LED chips have been mounted on heatsinks with indium solder. Since indium melts at a low temperature (156°C), lifetests at temperatures much over 90°C are not advisable, due to softening of the indium. Gold-tin (80/20) solder, which melts at 280°C, has recently been used to bond a group of LPE 1.3-µm LEDs. These were put up on lifetest at 120°C. Over 3000 h of undegraded operation have been accumulated to date. Based on these results, lifetests at 150°C will be initiated. These results again demonstrate the excellent reliability of InGaAsP devices and (together with other data in the literature [14]) suggest that mean times to failure comparable to Si devices (10^9 h) could be approached.

14. S. Yamasoshi, M. Abe, S. Komiya, and Y. Toyama, Tech. Digest IEEE IEDM Meeting, Washington, D.C., Dec. 1979, p. 122.

VIII. SUMMARY

This report describes research undertaken to optimize the device properties of 1.3-μm InGaAsP edge-emitting LEDs fabricated by both vapor-phase epitaxy (VPE) and liquid-phase epitaxy (LPE). In the previous final report (RADC-TR-80-110), details of the VPE growth process were given. Details of the LPE growth process are presented here. The LED efficiency of LPE devices was found to increase with decreasing cavity thickness. A value over 1% was measured with a 1000-Å cavity.

Contact stripe width and coupling technique were also varied to achieve maximum power into an optical fiber. The best coupling was obtained with a 12-μm-wide contact stripe. Significantly better coupling was also achieved with a balled, rather than cleaved, end fiber. More than twice the power could be coupled into a 100-μm core diam fiber, as compared to a 50-μm core fiber.

The temperature dependence of LED emission was also measured for both VPE and LPE devices. LED efficiency dropped over 30% between 20° and 70°C, while an emission wavelength shift of 5 to 6 Å/°C was observed over the same temperature range.

A summary of device properties is listed in Table 3. Comparable results have now been achieved with both LPE and VPE devices.

Highlights include typical coupled power into fibers of 40 μW (Best: 135 μW); spectral half-widths, ~600 Å; rise/fall times, ~3 ns; ac modulation rates, 100 to 200 MHz; and reliabilities (determined under separate government-sponsored programs) of >14,000 h @70°C (VPE) and >3000 h @ 120°C (LPE).

Far-field patterns from InGaAsP/InP were found to contain asymmetries due to the lack of absorbing substrate and cap layers. Some narrowing was achieved via the use of thin (1000 Å) active regions. Unusual effects upon far-field patterns were also observed when highly absorbing (i.e., low-bandgap) materials were incorporated into the device structures.

TABLE 3. SUMMARY OF DEVICE RESULTS FOR
InGaAsP/InP EDGE-EMITTING LEDs

	VPE		LPE	
	Typical	Best	Typical	Best
Power out (mW)	1.0	2.0	1.5	3.0
Power efficiency (@100 mA)	0.5	1.0	0.8	1.3
Power coupled into 50-μm GI* 0.2 NA fiber (μW)	40	135	40	120
Measured coupling efficiency	5%	13%	5%	11%
Spectral half-width (Å)	700	550	850	600
Rise/fall time (ns)	3	2.4	3	2.0
AC Modulation Rate (MHz @ 3 dB)	100	200	100	150
Reliability (still in progress)	high	<14,000 h @70°C	high	<3000 h @120°C

*Graded index.

41

REFERENCES

1. J. J. Hsieh, Appl. Phys. Lett. 28, 283 (1976).

2. D. Botez, IEEE J. Quantum Electron. QE-17 (1981).

3. D. Botez, Appl. Phys. Lett. 35, 57 (1979).

4. D. Botez, P. Zory and M. J. Brady, Elec. Lett. 14, 716 (1978).

5. D. Botez, IEEE J. Quantum Electron. QE-14, 230 (1978).

6. H. Burkhard and K. Mause, Solid State Electron. 21, 1551 (1978).

7. M. Ettenberg, H. Kressel, and J. P. Wittke, IEEE J. Quantum Electron. QE-12, 360 (1976).

8. D. Botez, RCA Review 39, 577 (1978).

9. Y. Seki, Jpn. Appl. Phys. 15, 327 (1976).

10. Y. Horikoshi, Y. Takanashi, and G. Iwane, Jpn. Appl. Phys. 15, 485 (1976).

11. H. Kressel and J. K. Butler, Semiconductor Lasers and Heterojunction LEDs, (Academic Press, NY, 1977).

'2. G. B. Thompson and G. D. Henshall, Electron. Lett. 16, 43 (1980).

13. Y. Horikoshi and Y. Furukawa, Jpn. J. Appl. Phys. 18, 809 (1979).

14. S. Yamasoshi, M. Abe, S. Komiya, and Y. Toyama, Tech. Digest IEEE IEDM Meeting, Washington, D.C., Dec. 1979, p. 122.
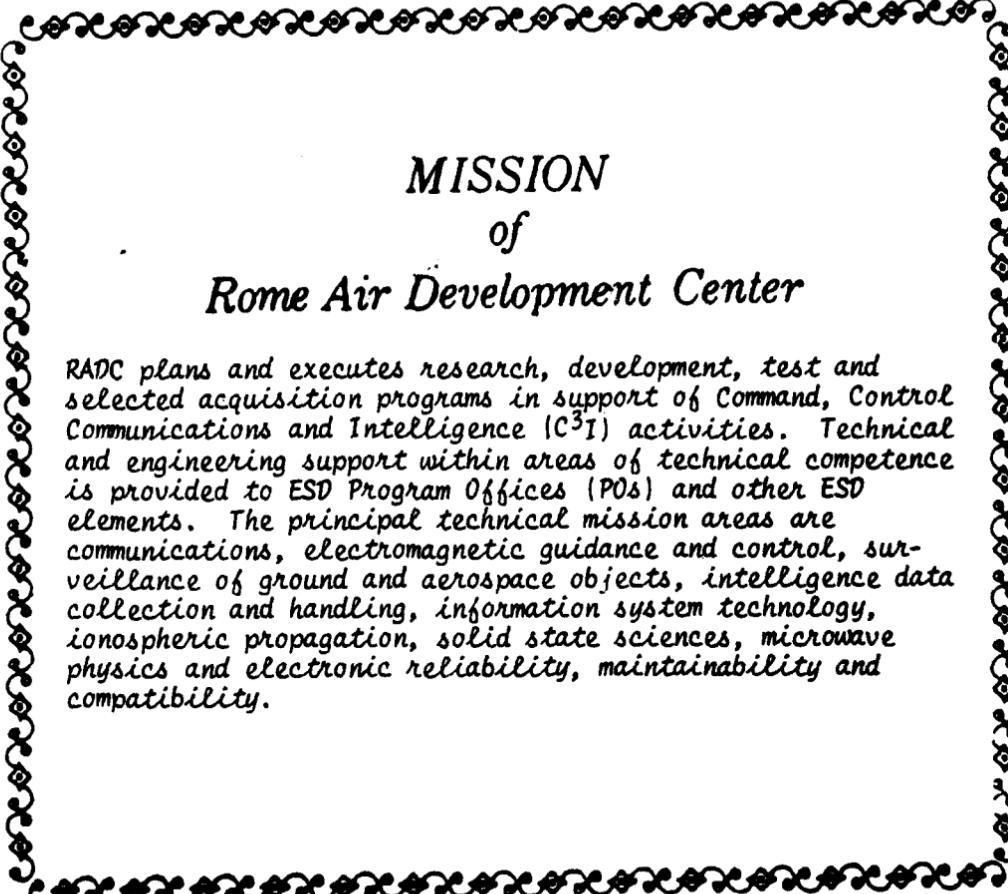
MISSION
of
Rome Air Development Center

RADC plans and executes research, development, test and selected acquisition programs in support of Command, Control Communications and Intelligence (C^3I) activities. Technical and engineering support within areas of technical competence is provided to ESD Program Offices (POs) and other ESD elements. The principal technical mission areas are communications, electromagnetic guidance and control, surveillance of ground and aerospace objects, intelligence data collection and handling, information system technology, ionospheric propagation, solid state sciences, microwave physics and electronic reliability, maintainability and compatibility.